A NOVEL APPROACH FOR THE SIMULATION OF MULTIPLE FLOW MECHANISMS AND POROSITIES IN SHALE GAS RESERVOIRS

A Thesis

by

BICHENG YAN

Submitted to the Office of Graduate Studies of
Texas A&M University
in partial fulfillment of the requirements for the degree of

MASTER OF SCIENCE

Chair of Committee,	John E. Killough
Committee Members,	Walter B. Ayers
	Yuefeng Sun
Head of Department,	A. Daniel Hill

August 2013

Major Subject: Petroleum Engineering

ABSTRACT

The state of the art of modeling fluid flow in shale gas reservoirs is dominated by dual porosity models that divide the reservoirs into matrix blocks that significantly contribute to fluid storage and fracture networks which principally control flow capacity. However, recent extensive microscopic studies reveal that there exist massive micro- and nano- pore systems in shale matrices. Because of this, the actual flow mechanisms in shale reservoirs are considerably more complex than can be simulated by the conventional dual porosity models and Darcy's Law. Therefore, a model capturing multiple pore scales and flow can provide a better understanding of complex flow mechanisms occurring in these reservoirs.

Through the use of a unique simulator, this research work establishes a micro-scale multiple-porosity model for fluid flow in shale reservoirs by capturing the dynamics occurring in three separate porosity systems: organic matter (mainly kerogen); inorganic matter; and natural fractures. Inorganic and organic portions of shale matrix are treated as sub-blocks with different attributes, such as wettability and pore structures. In the organic matter or kerogen, gas desorption and diffusion are the dominant physics. Since the flow regimes are sensitive to pore size, the effects of smaller pores (mainly nanopores and picopores) and larger pores (mainly micropores and nanopores) in kerogen are incorporated in the simulator. The separate inorganic sub-blocks mainly contribute to the ability to better model dynamic water behavior. The multiple porosity model is built upon a unique tool for simulating general multiple porosity systems in

which several porosity systems may be tied to each other through arbitrary transfer functions and connectivities. This new model will allow us to better understand complex flow mechanisms and in turn to extend simulation to the reservoir scale including hydraulic fractures through upscaling techniques.

DEDICATION

I dedicate this work to those people who have ever supported me throughout my life.

ACKNOWLEDGEMENTS

I would like to thank my committee chair, Dr. John E. Killough for being a father, mentor and friend to me. His wisdom and knowledge always inspire me, and I am honored to work with him.

I would like to thank Dr. Ayers and Dr. Sun, for their support and suggestions in my research work, and for serving as my committee members. I would like to thank my friend Yuhe Wang for the countless help with my research as a best group member. I would also like to thank my other group members and friends for their support.

I would like to thank Crisman Institute for the financial support to this research work. I would also like to thank Harold Vance Department of Petroleum Engineering for their support.

I would like to thank a lot of kind-hearted teachers and friends from China University of Petroleum (Beijing) for the support of my overseas study plan in every aspect before.

Finally, thanks to my family for their eternal support and encouragement and to my girlfriend Limin for her patience and love.

NOMENCLATURE

$\sum A_{mf}$	Total contact area between the matrix bulk and the fracture system, m^2
C_g	Gas compressibility, 1/Pa
D	Gas diffusion coefficient, m^2/second
d_{mf}	Nodal distance between the matrix bulk and the fracture system, m
g	Gravitational acceleration vector, m^2/s
GDC	Gas drainage capacity, kg/s/Pa
K	Media permeability, m^2
K_{app}	Apparent permeability within matrix, m^2
K_f	Fracture permeability, m^2
M_g	Gas Molecular weight, g/mole
N	Grid number
P	Pressure, Pa
$\overline{P}_f$	Average pressure in fracture, Pa
P_L	Langmuir pressure, Pa
$\overline{P}_m$	Average pressure in matrix bulk, Pa
q_a	Mass of gas adsorbed on unit volume of media, kg/m^3
q_f	Total rate flowing from matrix system into fracture system, kg/s
t	Time, second

TOC Weight Percentage of Total Organic Carbon, wt%

V_L Langmuir volume, m^3/kg

V_{std} Molar volume of gas at standard condition (273.15 K and 101.325 Pa), $m^3/mole$

z Distance in the gravitational direction, m

ρ_g Gas density, kg/m^3

ρ_{g_std} Gas density at standard condition (273.15 K and 101.325 Pa), kg/m^3

ρ_s Skeleton density of porous media, kg/m^3

μ_g Gas viscosity, Pa·second

$\overline{\mu}_{mf}$ Average gas viscosity in the micro-scale model, Pa·second

ϕ Porosity, dimensionless

δ Fracture aperture, m

TABLE OF CONTENTS

Page

LIST OF FIGURES

Page

Page

Page

LIST OF TABLES

Page

CHAPTER I

INTRODUCTION

1.1 Problem Statement

A major problem in simulation of gas flow in shale gas reservoirs is the existence of complex porosity systems. Those pore systems are in organic matter(kerogen), inorganic matter, natural fractures and hydraulic fractures (Wang and Reed 2009). The distribution of those different porosity systems is not well understood; a proper model beyond the traditional Dual Porosity or Dual Permeability Models is necessary to characterize the complex pore connectivities in shale gas reservoirs.

Another challenge in simulation of gas flow in shale gas reservoirs is the dominant physics occurring in such reservoirs. Shale gas reservoirs are unconventional because the gas storage and flow are controlled by multiple mechanisms. With a large quantity of nanometer-sized pores in shale, natural gas may be stored in terms of free gas as well as adsorbed gas. In such tight formations Darcy flow is insufficient to support significant gas flow, allowing diffusion and slippage flow to take on a more dominant role. Therefore, a well-designed model incorporating the dominant physical processes should add to our ability to evaluate the influences of different mechanisms on gas production in shale reservoirs.

The last issue is how to bridge mechanisms occurring at the micro-scale with a reservoir-scale model. Physics under small scales can be quantitatively analyzed, but the accuracy under macro-scales will be greatly reduced or even disappear without a proper

treatment. In shale gas reservoirs, there exist different fluid storage and flow mechanisms. Preservation of these dynamics in a macro-scale model is also important.

Most of the work about shale gas simulation available in the literature is focused on modeling the complexities of mechanisms in shale gas reservoirs or modeling shale gas through traditional Dual Porosity or Dual Permeability Models, yet neither cannot reasonably interpret the flow behavior of gas in shale. This study attempts to solve the above problems and it proposes novel approaches to characterize and simulate the complexities in shale gas reservoirs.

1.2 Background and Literature Review

The development of unconventional resource plays in North America has benefited from the technology advancements such as horizontal well drilling and hydraulic fracturing, and it has achieved great success towards satisfy the growing energy demand. The organic shale formations that provide the basis of much unconventional oil and gas production continue as an enigma as far as understanding production characteristics are concerned. Therefore, many investigators have been inspired to establish suitable models to characterize fluid flow in shale, encountering great challenges along the way.

Shale is referred to as extraordinarily fine-grained sediments commonly showing fissility (Javadpour 2009). Loucks et al. (2012) systematically classified nanometer- to micrometer-sized pores in the shale matrix into interparticle pores and intraparticle pores associated with mineral particles and organic-matter pores within kerogen, respectively.

The organic matter has different physical properties from common rock constituents and could significantly affect gas storage and flow in shale. Curtis et al. (2010) found that mostly kerogen is scattered in inorganic minerals, and pores within it are basically round in cross-section, interestingly, with numerous small pores residing on the interior walls of larger pores. Due to their formation during the process of hydrocarbon generation, the pore networks in the organic matter in shale are mainly considered to be oil- or gas-wet (Odusina et al. 2011; Wang and Reed 2009). Experiments on Barnett Shale demonstrated that the both adsorbed gas and free gas stored in the shale matrix are linearly increased with the Total Organic Carbon(TOC) content (Wang and Reed 2009), and Javadpour (2009) also theoretically proposed that in addition to free gas storage in shale, gas could also be adsorbed on the surface of kerogen and dissolved within it. Hill et al. (2000) estimated that between 20 and 85 percent of gas in shale might be stored as adsorbed gas. All those features make organic matter in shale unique and lead us to accept the proposal that the porosity systems in organic-rich shale could be separated into four types: inorganic bulk, organic matter, natural fractures, and hydraulic fractures (Wang and Reed 2009).

Due to the extremely low permeability (nano-Darcy scale) in the shale matrix, many investigators consider that Darcy flow is quite limited or even breaks down in shale with nanometer pore sizes. For this reason the validity of conventional dual porosity/permeability models has been frequently questioned.

Instead, the flow mechanisms in such tight formations have been re-investigated and many innovative methods have been proposed. The Dual-Mechanism Approach

(Darcy flow and Fickian diffusion occur simultaneously in matrix) was introduced to characterize the gas flow in coal or shale formations (Clarkson et al. 2012; Ertekin et al. 1986). Gas transport in such tight reservoirs is controlled by both pressure and concentration difference, and the effect of gas diffusion is considered as a dynamic gas slippage factor, which is composition, pressure and saturation dependent. Javadpour (2009) theoretically proposed the concept of apparent permeability through considering Knudsen diffusion, slippage flow and advection flow together, and the apparent permeability was further applied to pore scale modeling for shale gas (Shabro et al. 2011; Shabro et al. 2012). Based on a unified Hagen-Poiseuille-type formula (Beskok and Karniadakis 1999), Civan (2010) and Ziarani and Aguilera (2012) proposed a method to calculate apparent permeability through the intrinsic permeability of porous media and the flow condition function, which is a function of Knudsen number. The validity of this latter model for different flow regimes requires further confirmation. However, even with this greater detail, these models may not be sufficient, due to the use of an undivided shale matrix. Even with a proper connectivity between different pore systems there remains little understanding of this aspect (Andrade et al. 2011). On the other hand, Hudson et al. (2012) categorized the shale reservoir into organic porosity, inorganic porosity, natural fractures and hydraulic fractures, and explored several tank models for connections between each pore system. Unfortunately, the modes to characterize the distribution of each continuum and the connections between those continua appear too regular to be realistic for shale reservoirs. Clearly, there remains a strong requirement to accurately model production from unconventional reservoirs based

on detailed physics of the process and the interaction among to different pore systems such that modeling uncertainty is reduced.

1.3 Objectives and Procedures

Inspired by those predecessors and relying on the wide petrophysical knowledge about shale that is available in the literature, this study considers that conventional dual porosity/permeability models are not sufficient to describe those complex physics and dynamics. This research aims to establish a micro-scale model of shale gas reservoirs with several aspects.

(1) Due to the importance of organic matter in shale, TOC (Total Organic Carbon, wt%) will be an indispensable input parameter in the model.

(2) The shale matrix bulk will be strictly separated into inorganic matrix and organic matrix, and fractures will be located surrounding the matrix bulk as a constant pressure boundary.

(3) To further emphasize the organic matter in shale matrix, the existence of two types of porosity system distinguished in pore size in kerogen will be considered: organic matter with nanopores (average pore radii: 5 nm) and organic matter with micropores (average pore radii: 100nm).

(4) A well-designed algorithm that recognizes the random distribution and arbitrary connections between different continua will be introduced.

(5) Different mechanisms including Darcy flow, Fickian diffusion, free gas storage and Langmuir desorption will be considered in the micro-scale model.

(6) With the setup of this micro-scale model, the influences of those different mechanisms on the production of shale gas will be evaluated comprehensively.

(7) Finally, an upscaling approach to extend to the micro-scale model to a reservoir scale model will be proposed.

1.4 Organization of the Thesis

This study is divided into five Chapters. Its basic outline is shown as follows:

Chapter I briefly introduces the main challenges and the current methodologies to characterize gas flow in shale, and the main objectives and procedures to solve those problems in this research work;

Chapter II focuses on the motivation to establish the micro-scale model and model descriptions;

Chapter III mainly analyzes the influences of different mechanisms and important parameters on the gas production in shale, and also compares the micro-scale model with traditional Dual-Porosity model;

Chapter IV states a different methodology to upscale the micro-scale model to reservoir-scale model, and several real field cases are presented as well.

Chapter V finally concludes this research work, and provides some recommendations for future research.

CHAPTER II

MODEL DESCRIPTION*

2.1 Physical Model

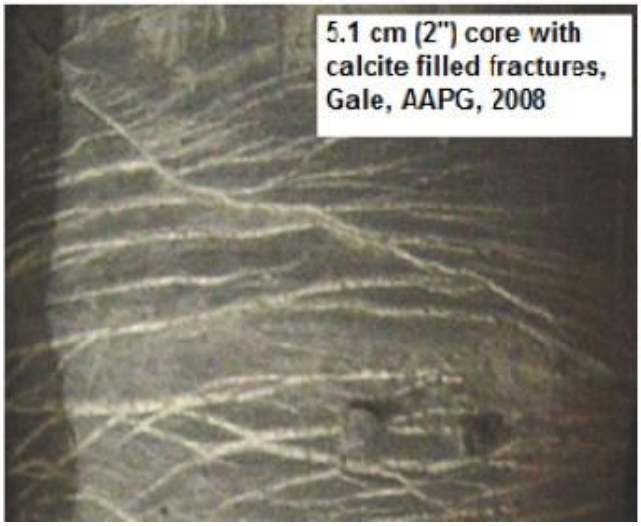

Fig. 2.1—Dense natural fracture development in shale (King 2010)

With the advances in experimental approaches, kerogen can be characterized as generally dispersed in inorganic minerals at the micrometer to nanometer scale. The width of natural fracture systems generally is less than 0.05 mm, as shown in Fig.2.1 (King 2010); therefore, the simulation scale should be limited to micrometers at most if subdivision of the shale matrix is required (Fig. 2.2).

* Reprinted with permission from "Beyond Dual-Porosity Modeling for the Simulation of Complex Flow Mechanisms in Shale Reservoirs" by Yan B., Wang Y., Killough J., 2013. Paper presented at the SPE Reservoir Simulation Symposium (RSS 2013). Copyright 2013 by SPE.

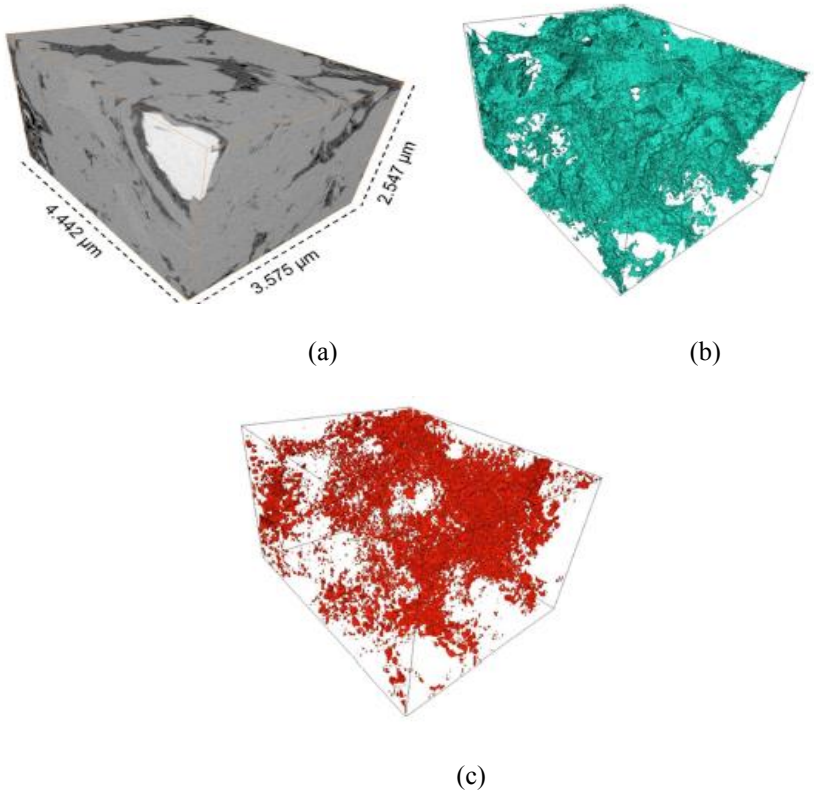

Fig. 2.2—Reconstruction of the Horn River sample (a) a 3-D matirx, (b) kerogen, (c) pore connectivity within matrix (Curtis et al. 2012).

Within a micrometer scale model, the interaction of the shale matrix and natural fractures can be sufficiently characterized. However, the validity of the micro-scale model work must be well-established before applying any upscaling approaches. Curtis et al. (2012) stated that in the shale matrix small pores (radii in 3 to 6 nm, hereafter referred to as "nanopores") predominate in the amount of pores but those larger pores (radii in 100 nm, hereafter referred to as "micropores") contribute most of the pore volume (Fig. 2.3). It is further proposed that the organic grids with nanopores could only connect to the organic grids with micropores. Therefore, any other pore systems in shale

should communicate with the organic matrix merely through those organic grids with micropores. This follows the observation from petrophysical data that in porous kerogen small pores penetrate the walls of larger pores (Fig. 2.4). Additional evidence indicates that the shale matrices are surrounded by natural fractures as pathways to connect with hydraulic fractures or the wellbore, and fractures are explicitly simulated with fine grids in the micro-scale.

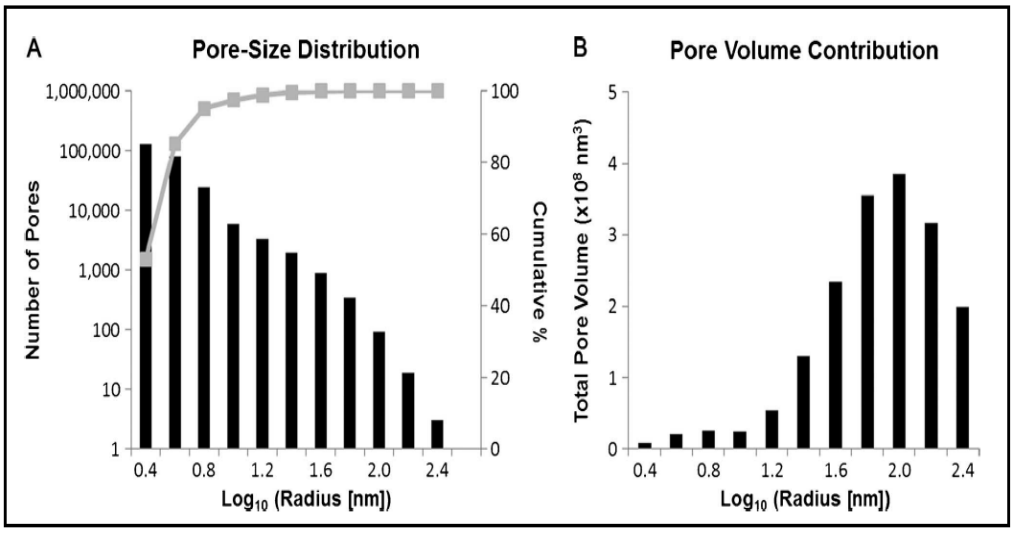

Fig. 2.3—(A) Pore-size distribution estimated from the Horn River reconstruction indicating that small pores dominate in number; (B) Volumetric contribution of the same pores with peak at 100 nm (Curtis et al. 2012).

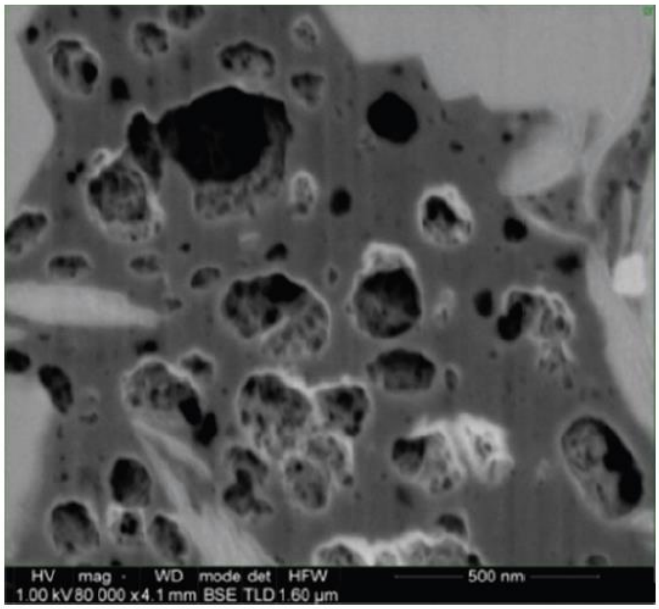

Fig. 2.4—BSE images of a region of kerogen with varying pore sizes (Curtis et al. 2010).

Therefore, there exist four different continua in the micro-scale model:

(1) Nano: organic matrix grid with nanopores with high porosity;

(2) Micro: organic matrix grid with micropores with high porosity as well;

(3) Inorg: inorganic matrix grid with very low porosity;

(4) Frac: natural fracture grid surrounding shale matrix grids to communicate with induced fractures and the wellbore.

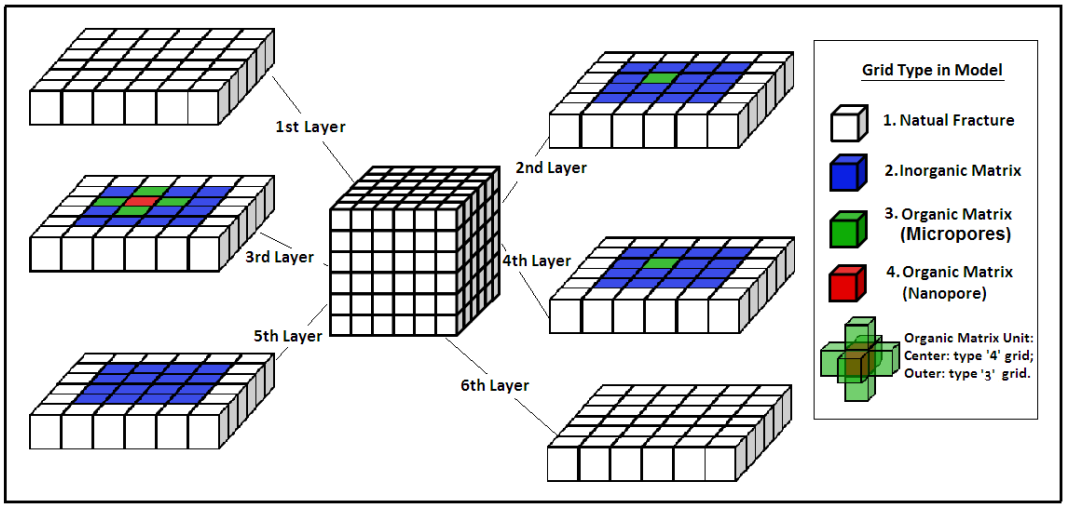

Fig. 2.5—Schematic of micro-scale multiple porosity model

The distribution and connections of those pore systems are a challenge for any simulation model. Because kerogen with nanopores has been assumed to be only connected to kerogen with micropores, in a Cartesian coordinate system, an organic matrix unit in the micro-scale model is designed such that one "Nano" cubic grid is surrounded by six "Micro" cubic grids on its six faces. A typical model with a single organic matrix unit is shown in Fig.2.5. This is a 6×6×6 grid system for instance, with one Organic Matrix Unit randomly distributed in shale matrix core surrounded by a layer of natural fracture grids.

Further, in the shale matrix the amount of those organic matrix units is controlled by the weight percentage of TOC and the properties of each medium from petrophysical data, shown as Equation (2.1), and the rest of the matrix grids are "Inorg" grids.

$$TOC = \frac{\rho_{micro} N_{micro}(1-\phi_{micro}) + \rho_{nano} N_{nano}(1-\phi_{nano})}{\rho_{micro} N_{micro}(1-\phi_{micro}) + \rho_{nano} N_{nano}(1-\phi_{nano}) + \rho_{inorg} N_{inorg}(1-\phi_{inorg})} \times 100\% \quad (2.1)$$

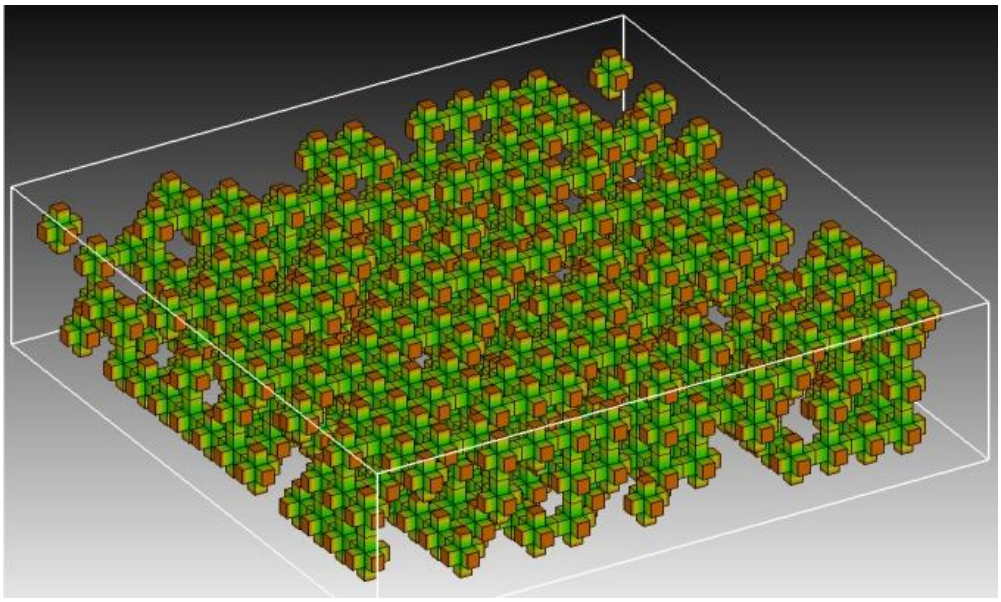

Fig.2.6—A sample mesh map for the micro-scale model with TOC 7.0 wt%

In order to achieve that kerogen grids could be dispersed within inorganic minerals, the locations of those organic matrix units are computed through a rigorous Monte Carlo Algorithm based on the grid number computed from Equation (2.1). Therefore, those organic grids (including “Micro” grids and “Nano” grids) and inorganic grids are randomly distributed within the shale matrix bulk. A sample mesh map based on the above algorithm is shown as Fig. 2.6. In Fig. 2.6, the cuboid is the matrix bulk, those green cross structures are actually the organic matrix units, and the empty space is for the inorganic minerals for a better resolution. From the figure it can be observed that organic grids are randomly distributed in the matrix bulk. Most of organic grids are well connected to each other. Some are isolated from others; however, generally the mesh map shows a great connectivity within the kerogen system making the mesh comparable to the physical map from Fig. 2.2.

2.2 Mathematical Model

Among the four continua listed above, in the inorganic minerals or fracture system, free gas is the only storage mechanism for gas. Besides, gas adsorption is assumed to only occur in organic grids (kerogen). Any pressure drop within the kerogen will induce gas molecules to be desorbed from the kergen surface. Therefore, the desorption process will actually increase the gas accumulation within the organic grids in this model. This phenomenon is taken into account in the simulator used in this work through terms of Langmuir isothermal function as Equation (2.2) (Civan et al. 2011; Cui et al. 2009; Freeman et al. 2012; Shabro et al. 2011).

$$q_a = \rho_s \frac{M_g}{V_{std}} \frac{V_L}{P_L + P} = \rho_s \rho_{g\_std} \frac{V_L}{P_L + P} \tag{2.2}$$

Because "Nano" grids can only connect to "Micro" grids as previously assumed, there are likely to be seven connections in total, shown as the following,

(1) $Micro \leftrightarrow Micro$

(2) $Micro \leftrightarrow Nano$

(3) $Micro \leftrightarrow Inorg$

(4) $Micro \leftrightarrow Frac$

(5) $Inorg \leftrightarrow Inorg$

(6) $Inorg \leftrightarrow Frac$

(7) $Frac \leftrightarrow Frac$

In those different connections, Fickian diffusion and Darcy flow is conditionally considered based on the actual flow mechanisms. In kerogen there are many nanopores

with small sizes very close to the size of methane molecule. Some investigators applied the Knudsen number to define the flow regimes and concluded that under such circumstances, conventional Darcy's law is problematic (Javadpour et al. 2007). For that reason it is assumed that free gas or desorbed gas flows across the connection between organic matter with nanopores and organic matter with micropores only through Fickian diffusion. Both Fickian diffusion and Darcy flow coexist in the connections between organic grids with micropores; however, there is only Darcy flow in any other connections elsewhere. From these assumptions it follows that a general formula of the mass balance equation for a single gas phase isothermal system can be written as follows(Yan et al. 2013a),

$$\nabla \cdot \left\{ \rho_g \left(DC_g \nabla P + \frac{K}{\mu_g} \left(\nabla P + \rho_g g \nabla z \right) \right) \right\} = -\frac{\partial (\rho_g \phi)}{\partial t} - \frac{\partial \left[q_a (1-\phi) \right]}{\partial t} \tag{2.3}$$

The first term in Equation (2.3) refers to the flux due to only Fickian diffusion, only Darcy flow or both mechanisms acting in parallel(Ertekin et al. 1986). The right hand side represents the accumulation of compressed gas in all of the grids as well as the accumulation of desorbed gas in organic grid blocks.

In the micro-scale model, Equation (2.3) is solved by a fully implicit iterative algorithm. Real gas properties are computed as a function of pressure under isothermal conditions through the Peng-Robinson equation of state in the model. There are natural fracture grids surrounding those matrix grids and set as a constant pressure boundary for the whole system. Therefore, gas in the shale matrix will spontaneously flow into the natural fracture system until the average pressure in the matrix decreases to the same

level of that in natural fracture system. Because the fracture grids are explicitly described in this model, the fracture permeability is related to fracture aperture as cubic law (Hoteit and Firoozabadi 2006).

$$K_f = \frac{\delta^2}{12} \tag{2.4}$$

2.3 Conclusions

This chapter presents a micro-scale model with quad-porosity for shale gas reservoirs. The model is linked with petrophysical data through the TOC content. The connections between different porosity systems are approached through arbitrary connectivities in a random grid system. Further, mechanisms including Darcy flow, Fickian diffusion, and Langmuir desorption are included in the model.

CHAPTER III

RESULTS ANALYSIS*

3.1 Introduction

The dimensions of the micro-scale system are 482 μm ×482 μm ×92 μm divided into 50 grids ×50 grids ×11 grids, in total 27,500 grids. Generally, the length of each matrix cub is 10 μm and the fracture aperture is 1 μm. The TOC value is typically 12.50 wt%, and other media properties are presented in Table 3.1 below. Note that the mesh data, TOC content and data in Table 3.1 are used in the following parts of this section as the default if not specified. Based on Equation (2.1) the organic grid number is 5243 (the ratio of the "Micro" grid number to the "Nano" grid number is constantly 6:1). Because the gas mass within such a fine scale model is in the magnitude of 10^{-10} kg, the drainage process is very short (0.001 to 0.1 seconds) and at the later period of the drainage process the gas in place is an important constraint on gas drainage rate. Therefore, to better compare the significance of different mechanisms on gas flow, a parameter analogous to "Productivity Index" is defined here, which is now called as "Gas Drainage Capacity into the Fracture System (GDC)".

$$GDC = \frac{q_f}{\overline{P}_m - \overline{P}_f} \tag{3.1}$$

* Reprinted with permission from "Beyond Dual-Porosity Modeling for the Simulation of Complex Flow Mechanisms in Shale Reservoirs" by Yan B., Wang Y., Killough J., 2013. Paper presented at the SPE Reservoir Simulation Symposium (RSS 2013). Copyright 2013 by SPE.

3.2 Effect of Desorption

To evaluate the effect of the gas desorption in kerogen on gas flow in shale, diffusion in the kerogen is temporarily deactivated such that Darcy flow is the only flow mechanism. The Langmuir pressure for both "Micro" and "Nano" grids are taken as 1,500 psi (Hudson et al. 2012), and with a different Langmuir volume of methane in the kerogen, the adsorption isotherm curve can be changed significantly causing the corresponding Adsorbed Gas Weight Percentage (hereafter referred to as "AGWP") to vary. To reasonably analyze the effect of desorption, the AGWP value should be controlled within a realistic range. All parameters in Table 3.1 are applied here and Table 3.2 lists the Langmuir adsorption parameter of different organic grids for five different cases.

Table 3.1—Description of medium properties for the micro-scale modeling

Medium Type	"Frac"	"Inorg"	"Micro"	"Nano"
Media Density(g/cc)	----	2.6	1.35	1.40
Media Porosity	1.00	0.02	0.2	0.25
Media Permeability (mD)	84.40	5.0×10^{-5}	5.0×10^{-5}	0.0
Media Pressure (MPa)	8.6	17.2		
Media Temperature (K)	373.15			

Note the density of inorganic bulk and organic matter in shale is estimated from Passey et al. (2010).

Fig. 3.1 compares the cumulative gas rate curves for the five cases. The figure shows that in the early period of the gas drainage process, there is little difference among those cases because initially free gas in the pores mainly supports the gas drainage.

However, at the later period of time, the effect of desorption in kerogen becomes significant so that the cumulative gas rate could increase with increasing AGWP. Using Case 1 without desorption as a base case, the increase of the ultimate cumulative gas rate into the natural fracture system for Cases 2 to 5 is 10.3%, 13.47%, 16.62% and 19.77% respectively.

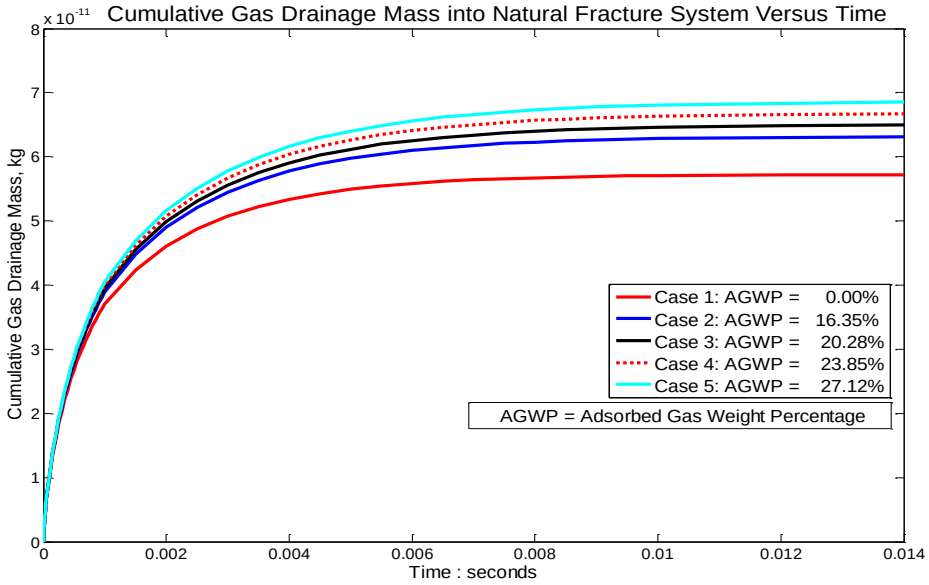

Fig. 3.1—Cumulative gas rate curves for five cases with different adsorbed gas weight percentage

Fig. 3.2 exhibits the change of average pressure in the matrix bulk with time. The effect of desorption helps to maintain the pressure within the matrix bulk, but not substantially. It is worth to note that since in this model it is assumed that there is no Darcy flow within the Organic "Nano" grids and with here diffusion nullified as well,

the average pressure will not decline to the level in the fracture grids during the period simulated.

Table 3.2—Adsorption parameters for each case to evaluate desorption in shale (no diffusion)

Case NO.	V_L in Micro (scf/ton)	P_L in Micro (psi)	V_L in Nano (scf/ton)	P_L in Nano (psi)	AGWP (%)
1	0	0	0	0	0.00
2	325	1500	375	1500	16.35
3	425	1500	475	1500	20.28
4	525	1500	575	1500	23.85
5	625	1500	675	1500	27.12

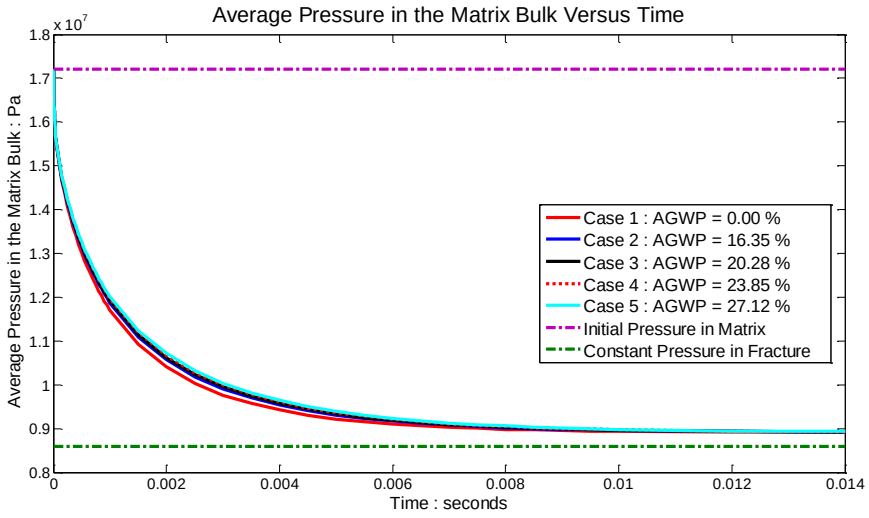

Fig. 3.2—Average pressure curves for five cases with different adsorbed gas weight percentage

Fig. 3.3 compares the curves of gas drainage capacity (defined in Equation (3.1)) with time in a semi-log plot for the five cases, and through calculation it shows that

during the range of 0 to 0.004 seconds, on average 90% of total producible gas is drained into fracture system. Desorption only improves gas drainage capacity maximally about 16.7% (in Case 5 with AGWP = 27.12%). Therefore, desorption increases gas drainage capacity during the later times but its influence is not considerable; the main contribution of desorption to gas production in shale is that it increases the cumulative gas rate from shale after pressure starts depletion. This is caused by the adsorption model applied here and the way it affects the gas flow in shale. As part of accumulation term and with the same unit as gas density, q_a in Equations (2.2) and (2.3) should be evaluated in a time or pressure scale similar to gas density, which is,

$$\frac{\partial q_a}{\partial t} = \frac{\partial}{\partial P}(\rho_s \rho_{g\_std} \frac{V_L P}{P_L + P}) \frac{\partial P}{\partial t} = \rho_s \rho_{g\_std} \frac{V_L P_L}{(P_L + P)^2} \frac{\partial P}{\partial t} \tag{3.2}$$

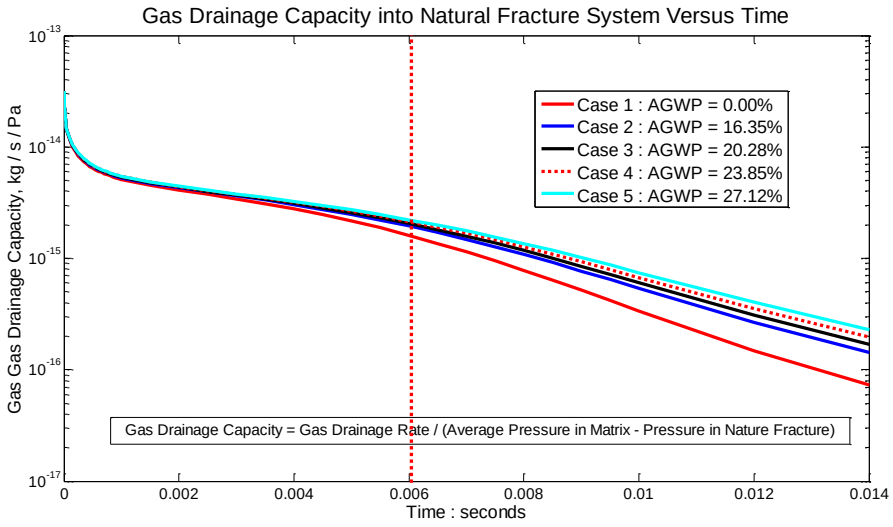

Fig. 3.3—Gas drainage capacity curves for five cases with different adsorbed gas weight percentage

Equation (3.2) implies that as pressure decreases with producing time, the effect of desorption on gas accumulation in kerogen increases significantly with given properties in the system and pressure drop.

3.3 Effect of Diffusion

To better evaluate the effect of diffusion, the Langmuir adsorption parameters are set to zero so that only free gas resides in shale matrix. The mesh system and the parameters listed in Table 3.1 are still used. According to Hoteit et al. (2006), the diffusion coefficient in gas phase is in the range of 8.7×10^{-4} m^2/sec, so the gas diffusion coefficients of organic grids are here set in the range of 10^{-8} to 10^{-4} m^2/sec to conduct the sensitivity analysis. In a fashion similar to the analysis of desorption process, if the diffusion coefficient in the "Nano" grids is zero, gas within those grids cannot be drained out and the average pressure in the matrix cannot reach the pressure in the fracture system outside. **Table 3.3** enumerates the diffusion coefficients in organic grids for five cases. Note that diffusion is hypothesized to only occur in kerogen.

Table 3.3—Diffusion coefficients for each case to evaluate diffusion in kerogen (no desorption)

Case NO.	Dv (Diffusion Coefficient in "Vug") (m^2/sec)	Dn (Diffusion Coefficient in "Nano") (m^2/sec)
6	0.00	0.00
7	7.09×10^{-7}	4.43×10^{-8}
8	7.09×10^{-6}	4.43×10^{-7}
9	7.09×10^{-5}	4.43×10^{-6}
10	7.09×10^{-4}	4.43×10^{-5}

Fig. 3.4 shows the relationship of cumulative gas rate into the fracture system with time. The comparison shows that there is little difference in the ultimate cumulative gas rate for those cases considering diffusion. The greater the diffusion coefficients the faster the cumulative rate curves reach the peak level. As previously claimed, without considering diffusion the gas stored in "Nano" grids can never be produced. Comparing to the ultimate cumulative rate of Case 7 to 10, there is a significant decrease of about 15% on average of that in Case 6 (base case) which neglects diffusion in kerogen. In **Fig. 3.5**, the above observations could be further confirmed: diffusion could accelerate the pressure drop within the matrix bulk, and Case 6 consequentially maintains a little higher average pressure because of more gas left in those "Nano" grids. Finally, in **Fig. 3.6** it can be concluded that diffusion greatly increases the gas drainage capacity into fracture system, especially at the later time of production or at a lower average pressure in shale matrix.

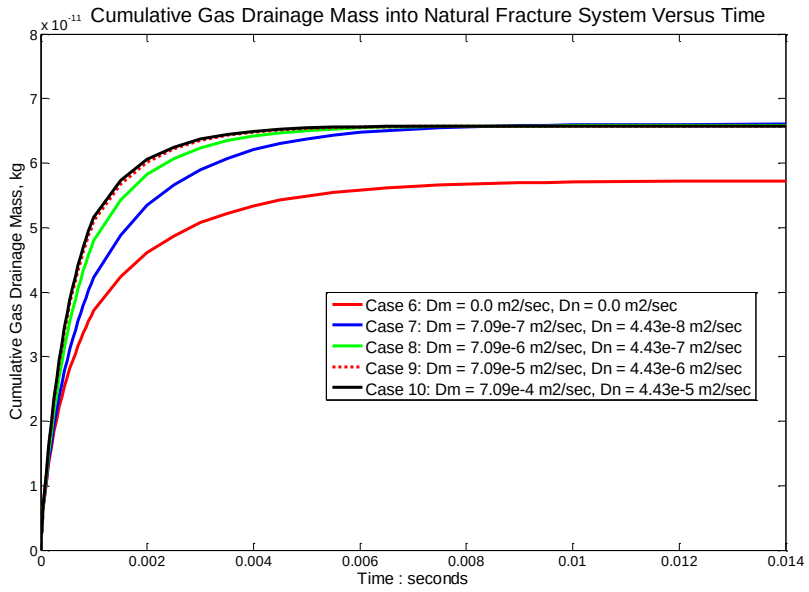

Fig. 3.4—Cumulative rate curves for cases with different diffusion coefficients in kerogen

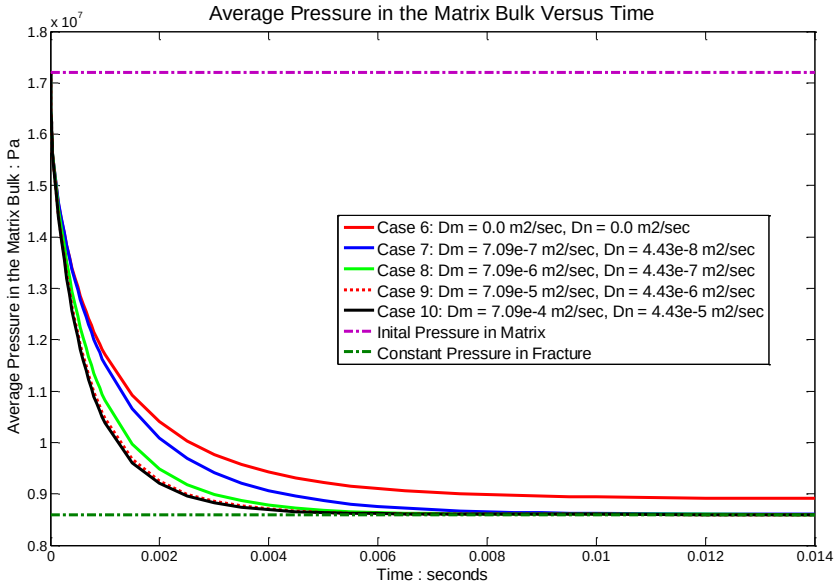

Fig. 3.5—Average pressure curves for cases with different diffusion coefficients in kerogen

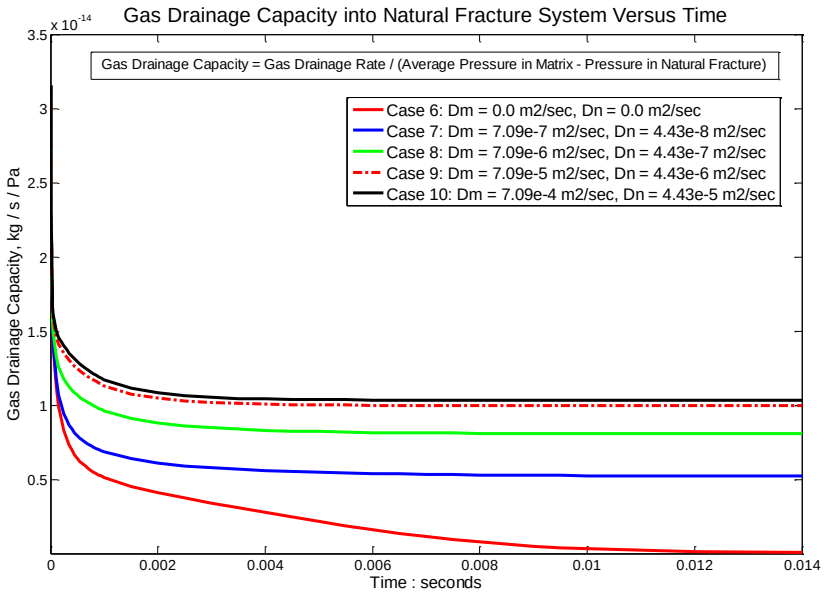

Fig. 3.6—Gas drainage capacity curves for five cases with different diffusion coefficients in kerogen

3.4 Comparison with Dual Porosity Model

With the same mesh system as above, a Dual Porosity Model with homogeneous matrix grids is established to compare with the Micro-Scale Model considering diffusion and desorption, and still keep the initial pressure in matrix bulk at 17.2 MPa, pressure in fracture system constant at 8.6 MPa and temperature in the system constant at 373.15 Kelvin. **Tables 3.4** through **3.6** list the parameters related to each medium in each case.

Table 3.4—Parameters for dual porosity model (AGWP: 0.00%)

Medium Type	Natural Fracture	Shale Matrix
Media Density(g/cc)	----	2.20
MediaPorosity(fraction)	1.00	6.73%
Media Permeability(mD)	84.40	5.0×10^{-5}
Media Diffusivity (m^2/sec)	0.00	0.00

Note: the pore volume in the Dual Porosity Model is the same as that in the Micro-Scale Model.

Table 3.5—Parameters for the micro-scale model considering diffusion (AGWP: 0.00%)

Medium Type	"Frac"	"Inorg"	"Micro"	"Nano"
Media Density(g/cc)	----	2.60	1.35	1.40
Media Porosity(fraction)	1.00	2.0%	20.0%	25.0%
Media Permeability(mD)	84.40	5.0×10^{-5}	5.0×10^{-5}	0.00
Media Diffusivity (m^2/sec)	0.00	0.00	7.09×10^{-5}	4.43×10^{-6}

Table 3.6—Parameters for the micro-scale model considering diffusion and desorption (AGWP: 18.36%)

Medium Type	"Frac"	"Inorg"	"Micro"	"Nano"
Media Density(g/cc)	----	2.60	1.35	1.40
Media Porosity(fraction)	1.00	2.0%	20.0%	25.0%
Media Permeability(mD)	84.40	5.0×10^{-5}	5.0×10^{-5}	0.00
Media Diffusivity (m^2/sec)	0.00	0.00	7.09×10^{-5}	4.43×10^{-6}
Langmuir Volume(scf/ton)	0.00	0.00	375	425
Langmuir Pressure(psi)	0.00	0.00	1500	1500

Fig. 3.7 shows the cumulative gas rate flowing into natural fracture system for each case. With the same gas in place, the Micro-Scale Model only considering diffusion could reach the cumulative rate plateau much earlier than Dual Porosity Model, and the

ultimate gas recovery is almost the same. The Micro-Scale Model considering both diffusion and desorption could have on average 12.0% more ultimate cumulative gas rate than those of another two cases. The deviations of these three curves also indicate that Darcy flow, diffusion and desorption occur sequentially in the micro-scale model.

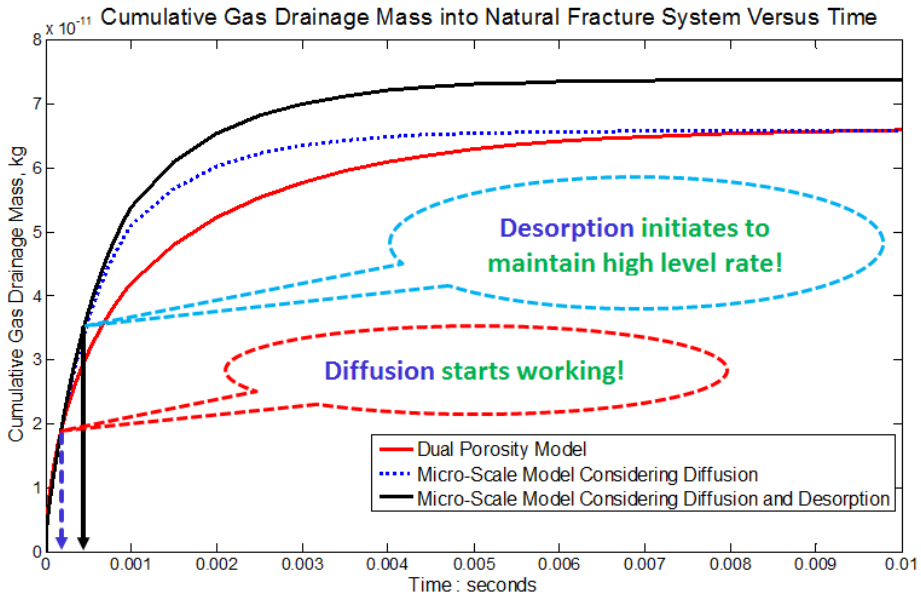

Fig. 3.7—Cumulative gas rate curves to compare micro-scale model with conventional dual porosity model

In **Fig. 3.8**, the two Micro-Scale Models only cost almost half of the time to decrease the average pressure in the matrix bulk to the pressure in fracture system comparing to the conventional Dual Porosity Model, and the desorption in the kerogen could moderately maintain the pressure in the matrix bulk.

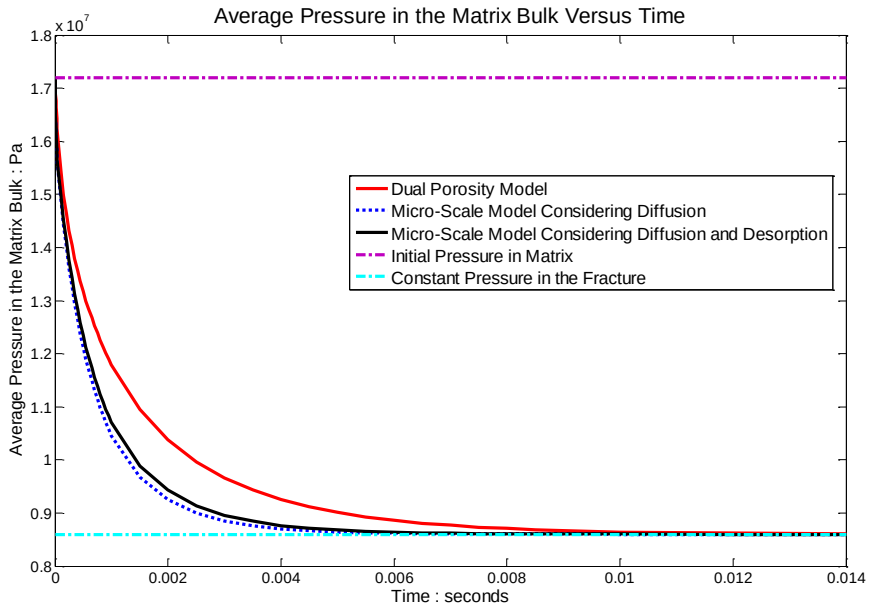

Fig. 3.8—Average pressure curves to compare micro-scale model with conventional dual porosity model

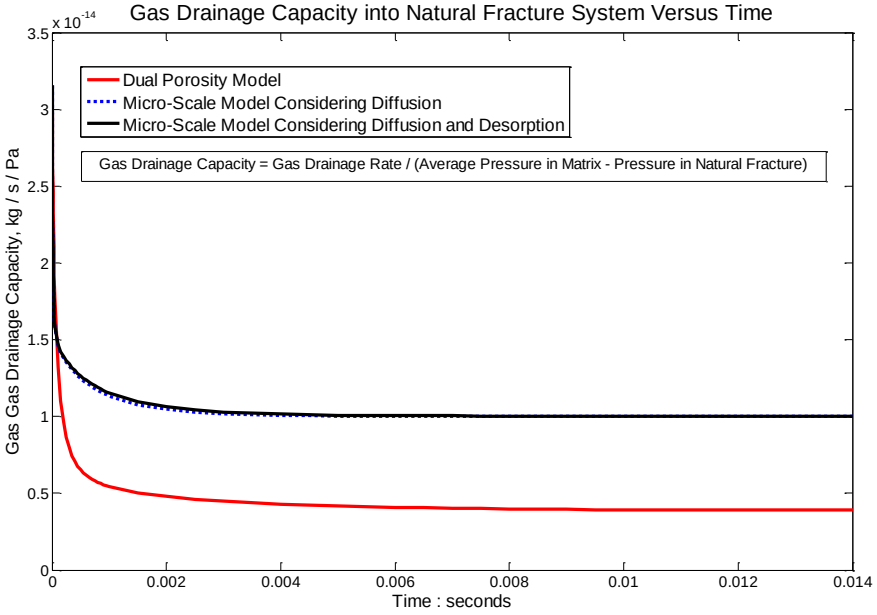

Fig. 3.9—Gas drainage capacity curves to compare micro-scale model with conventional dual porosity model

Fig. 3.9 exhibits the curves of gas drainage capacity changing with time for the three models, and it is very clear that through diffusion the Micro-Scale Model maintains a much greater gas drainage capacity than the Dual Porosity Model, and desorption actually has little or even no effect to increase this parameter.

3.5 Effect of Organic Grids (Kerogen) Distribution in Shale Matrix

To obtain an obvious effect of the random distribution for the organic grids, here TOC content in the shale matrix is set constant at 7.0% (constant number of organic grids). However, the dimensions of the system are still 482 μm ×482 μm ×92 μm divided into 50 grids ×50 grids ×11 grids, with fracture aperture 1 μm and matrix cube length 10 μm; in the system the temperature is constant at 373.15 Kelvin, the initial pressure in the matrix bulk is 17.2 MPa and the pressure in natural fracture system maintains at 8.6 MPa. Other parameters related to each medium are from Table 3.6, but because of the lower TOC content here, the AGWP is now decreased to about 15.8%. Five mesh systems (Case 11 to 15) with different kerogen random distribution (different random seed for each case) are generated and coupled into the simulator.

Fig. 3.10 to **Fig. 3.12** respectively show the cumulative gas rates into the natural fracture system, the average pressure in the matrix bulk and the gas drainage capacity for the five cases. From these figures, it can be observed that the five series of curves overlap completely. The maximum differences between the five cases for the three different plots are respectively 0.19%, 0.0252% and 0.3%, which can be almost

neglected. Therefore, it is concluded that the random distribution modes of kerogen with a given TOC value cannot impact the global gas flow behavior in shale.

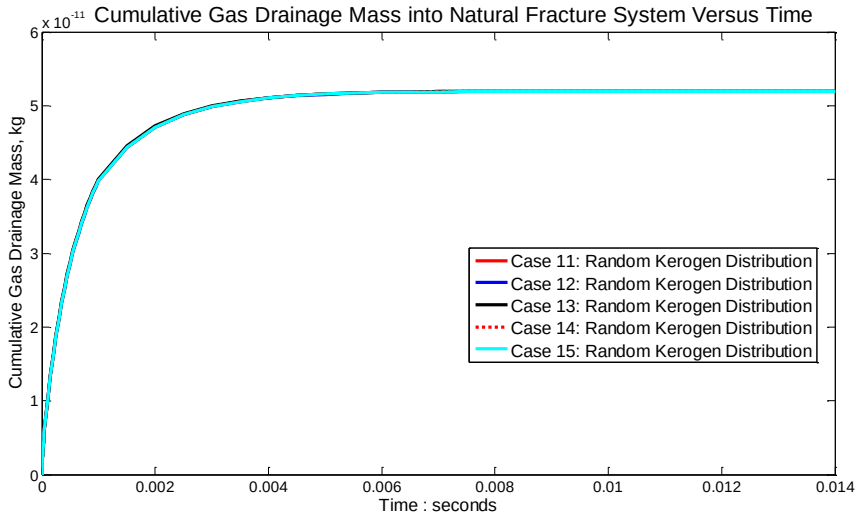

Fig. 3.10—Cumulative gas rate curves for five cases with different kerogen distribution modes

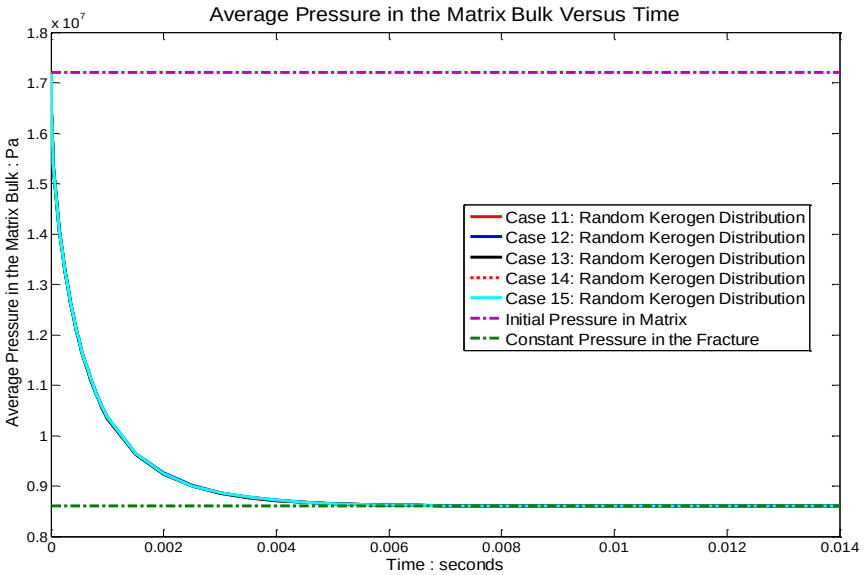

Fig. 3.11—Average pressure curves for five cases with different kerogen distribution modes

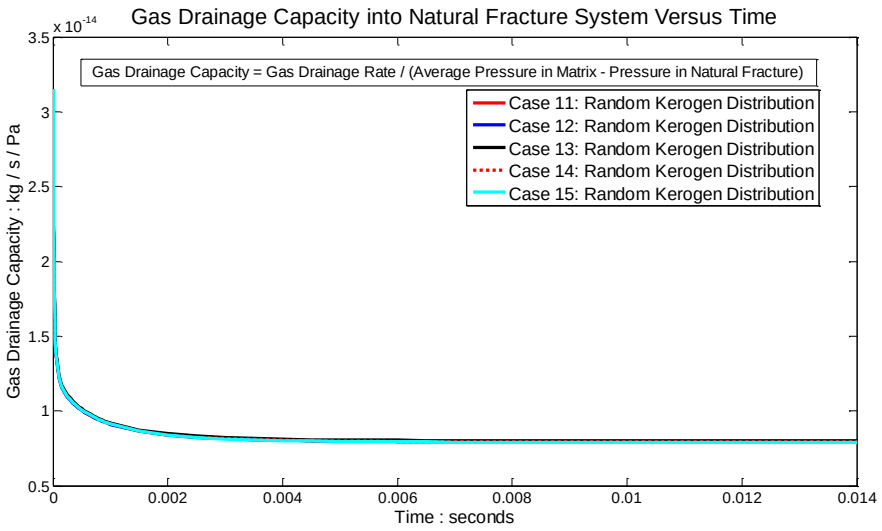

Fig. 3.12—Gas drainage capacity curves for five cases with different kerogen distribution modes

Fig. 3.13 is a sample matrix grids map in each layer for Case 11. The organic grids (white grids) are randomly distributed within the inorganic grids (black grids), and in space it is like a cluster of kerogen evenly distributed within the inorganic minerals. Moreover, a pressure map for the matrix bulk corresponding to this mesh map is shown in **Fig. 3.14**. Through comparison of the two maps, the pressure map matches perfectly with the distribution of organic grids. In the pressure maps of layers 4, 5 and 6 in the matrix, which are actually the inner part of the matrix bulk in a three dimensional view, the pressure within organic grids (shallow red) are on average lower than that of inorganic grids (dark red) because of the well developed and connected kerogen system compared to inorganic minerals nearby. However, in pressure maps of other matrix layers which are the outer part the shale matrix, the pressure in organic grids is much higher than that in inorganic grids. This is partly because of the desorption effect in

kerogen and partly because of the poor connectivity of kerogen at the tail end of the kerogen cluster compared to that of the inner organic grids.

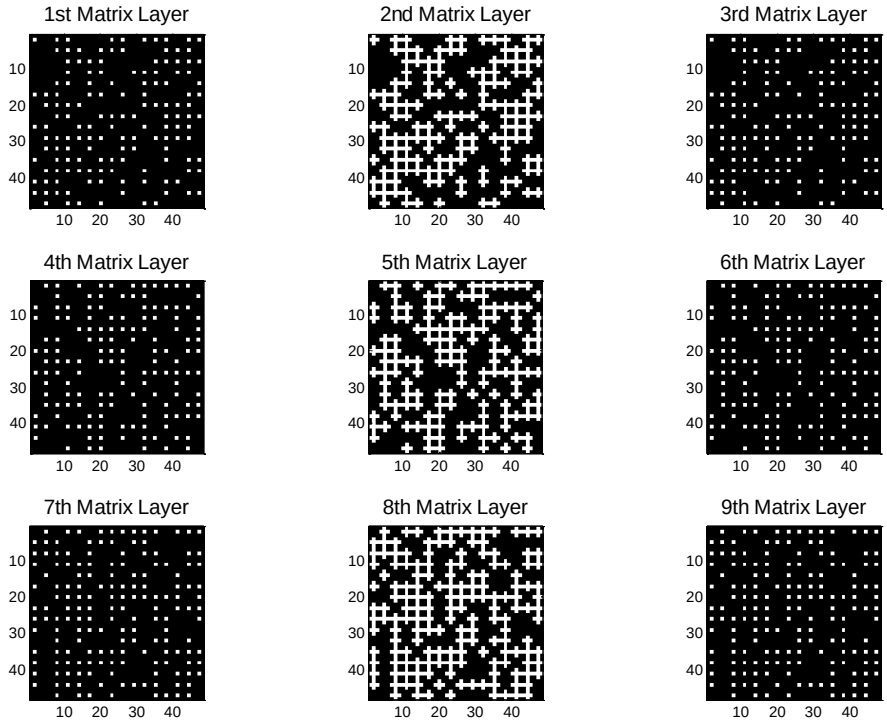

Fig. 3.13—Matrix grids map distribution for 9 layers of matrix in Case 11 with TOC 7.0 wt%

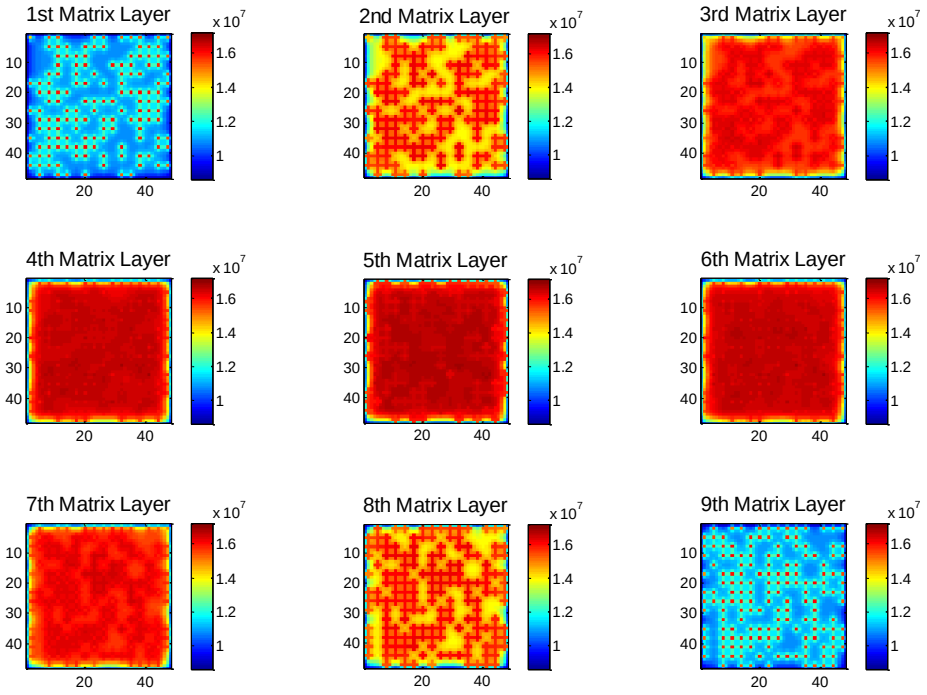

Fig. 3.14—Pressure map for 9 layers of matrix in vertical direction

3.6 Effect of TOC Content in Shale Matrix

Here typical TOC values 3.00 wt% (Case 16), 6.00 wt% (Case 17) and 12.00 wt% (Case 18) are used to show the difference of simulation results. Still the dimensions the system are kept at 482 μm ×482 μm ×92 μm divided into 50 grids ×50 grids ×11 grids, with fracture aperture 1 μm and matrix cub length 10 μm; in the system the temperature is constant at 373.15 Kelvin, the initial pressure in the matrix bulk is 17.2 MPa and the pressure in natural fracture system maintains at 8.6 MPa. Besides, the parameters in **Table 3.6** for each medium are still applied. Under the initial condition in

the system, the AGWP in shale matrix are respectively 11.09%, 15.00% and 18.21% for the three cases with an increase trend in TOC content.

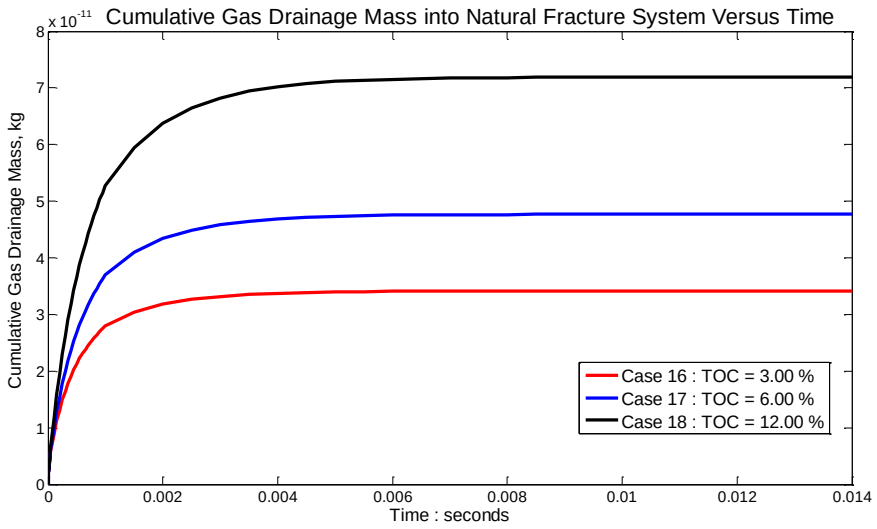

Fig. 3.15—Cumulative gas rate curves for cases with different TOC value

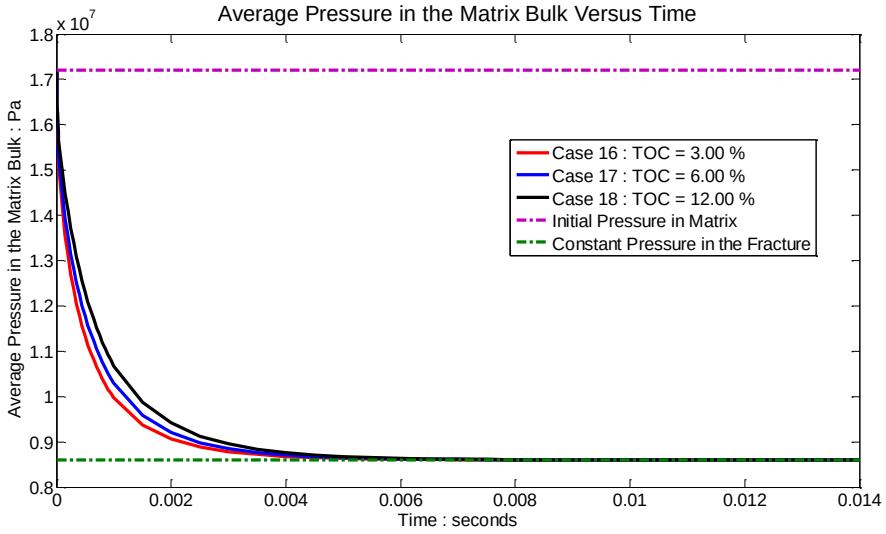

Fig. 3.16—Average pressure curves for cases with different TOC value

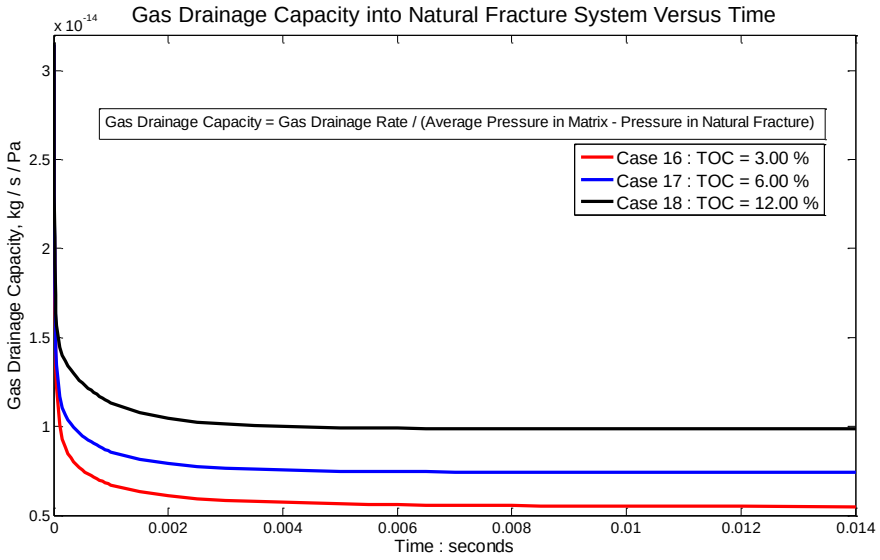

Fig. 3.17—Gas drainage capacity curves for cases with different TOC value

Fig. 3.15 to **Fig. 3.17** show those curves of the cumulative gas rate, average pressure within the matrix bulk and gas drainage capacity into the fracture system versus time for Case 16 to 18. From those curves, it could be observed that higher TOC content in shale matrix will lead to greater ultimate cumulative gas production, lower speed to decrease the average pressure in matrix bulk and significantly higher gas drainage capacity. Kerogen has considerable gas adsorption capacity and much higher porosity than that of inorganic minerals. In consequence, an increase in TOC could directly bring more gas in place to sustain higher gas drainage rate. Case 17 (6.00 wt% TOC) and Case 18 (12.00 wt% TOC) could respectively ultimately release 1.4 and 2.1 times more gas into the fracture system than Case 16 (3.00 wt% TOC). Meanwhile, because of greater gas in place for cases with higher TOC content, to keep mass conservative the average pressure in matrix bulk stays slightly higher (**Fig. 3.16**). Moreover, diffusion could only

occur in the organic matrix and thus an increase in TOC value will magnify the gas drainage capacity due to the significantly increasing effect of diffusion in kerogen, which is exhibited in **Fig. 3.17**.

3.7 Conclusions

With the setup of the micro-scale model, this chapter analyzes the influences of main mechanisms on gas flow in shale in the micro-scale model. Desorption increases gas in place but has little to do with the gas drainage capacity; however, diffusion greatly enhances gas flow capacity but not ultimate gas recovery. The comparison between the micro-scale model and Dual Porosity Model shows that other mechanisms besides Darcy flow cannot be neglected. Further, it also demonstrates that the random distribution of kerogen grids is a reasonable approach to characterize kerogen distribution in shale. Finally, because TOC controls the weight percentage of organic carbon in shale, the effect of TOC on gas production in shale is through a superposition of both diffusion and desorption occurring in kerogen.

CHAPTER IV

UPSCALING METHOD*

4.1 Apparent Permeability

The comprehensive work in the previous session is limited in micro-scale simulation for qualitative analysis. It could not be used for reservoir scale simulation unless it is upscaled. Besides, the scale so far is within the range of a matrix bulk subdivided by tens of thousands of gridblocks surrounded by natural fracture grids outside; therefore, it is a transient behavior we could observe. To make the work friendly to commercial simulators, here the apparent permeability (K_{app}, shown in Equation (4.1)) is calculated for the system similar to Darcian permeability, which is now approximated as an average behavior within the matrix bulk considering the different mechanisms coupled in the micro-scale model(Yan et al. 2013b; Yan et al. 2013a),

$$K_{app} = \frac{q_f d_{mf} \bar{\mu}_{mf}}{(\bar{P}_m - \bar{P}_f)\sum A_{mf}} \tag{4.1}$$

In this part, TOC content in shale matrix is set constant as 10.0 wt%. The dimensions of the model are divided into 32 grids × 32 grids × 32 grids, with 5268 organic grids and 32,678 grids in total. Organic grids are randomly distributed within matrix and fracture grids encircle the matrix cubic bulk. Fracture aperture is constantly set as 1 μm, but the size of matrix grid is varied from 10 μm to 1 m. Initial pressure in

* Reprinted with permission from "Beyond Dual-Porosity Modeling for the Simulation of Complex Flow Mechanisms in Shale Reservoirs" by Yan B., Wang Y., Killough J., 2013. Paper presented at the SPE Reservoir Simulation Symposium (RSS 2013). Copyright 2013 by SPE.

matrix is set as 17.2 MPa, and pressure in natural fracture is 8.6 MPa, with temperature 373.15 Kelvin everywhere in the system. Medium properties are from **Table 3.6**, but diffusion coefficients or Langmuir Parameters are respectively nullified to analyze the effect of diffusion, desorption and Darcy flow on apparent permeability in Equation (4.1).

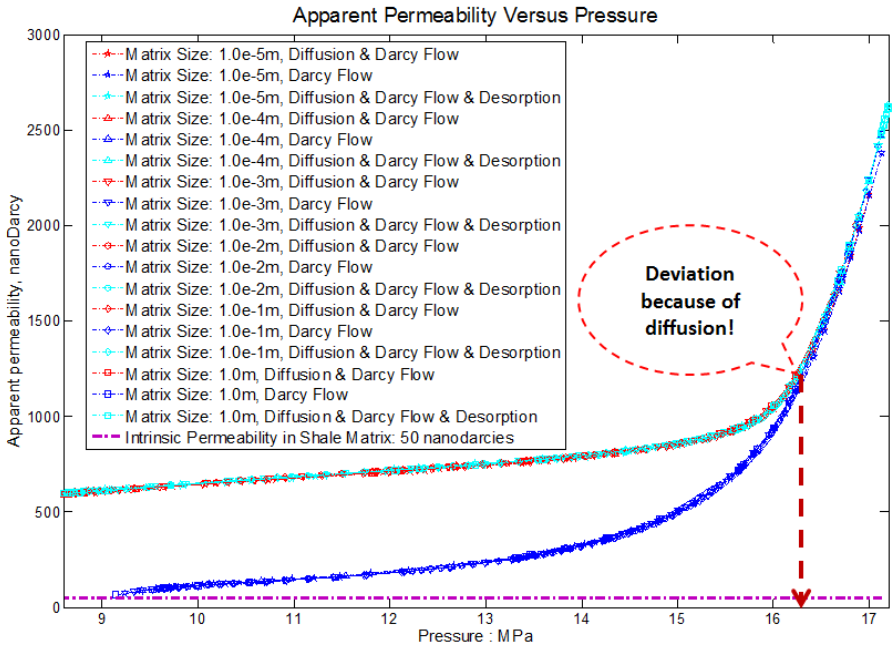

Fig. 4.1—Apparent permeability as a function of pressure with different matrix grids size

Three series of cases with different matrix size are simulated through the micro-scale model, and the results are plotted in **Figs. 4.1** and **4.2**. In **Fig. 4.1**, at the early period of pressure drop, the apparent permeability of those different cases are almost overlapped because of the domination of Darcy flow in the system; gradually those cases

considering diffusion would maintain a much higher K_{app} than the cases neglecting diffusion which finally decline to the level of the intrinsic permeability (50 nanoDarcies) within the "Micro" or "Inorg" grids. On the other hand, desorption does not affect the apparent permeability at all because there is no difference between cases considering desorption and diffusion and cases considering diffusion. The results depicted in Fig. 4.1 also indicate that matrix size does not change the apparent permeability in any cases plotted. This sets a solid foundation to extend the previous micro-scale model to a reservoir model later. In **Fig. 4.2**, the apparent permeability ratio of cases considering diffusion (and desorption) to cases only considering Darcy flow increases with the pressure decrease in the matrix cube bulk. The results are comparable to the results of the tube model considering Knudsen diffusion, advection and slip flow from Javadpour (2009). Meanwhile, it further demonstrates that desorption has neglectable effect on the apparent permeability through the comparison of the two cases in **Fig. 4.2**.

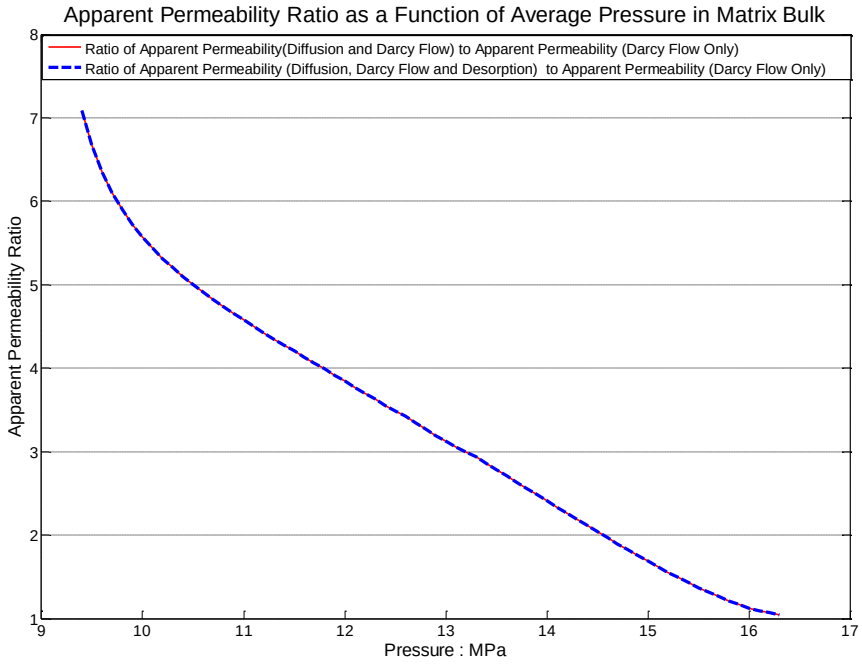

Fig. 4.2—Apparent permeability ratio (base case: Darcy flow only) as a function of pressure

To exclude the likelihood that the apparent permeability is dominated by the fixed natural fracture permeability above, here the effect of fracture permeability on the apparent permeability is analyzed. Based on the smallest model (matrix grid size: 10 μm and fracture grid size: 1 μm) when evaluating the apparent permeability considering diffusion, Darcy flow and desorption, here the fracture permeability is changed from 0.844 mD to 8.44 D with any parameters else in the system the same. The result of the apparent permeability is shown in **Fig. 4.3**. As shown in the figure, with five fracture permeabilities in significantly different magnitudes, the curves for apparent permeabilities versus pressure have no difference and overlap one another. Therefore, the permeability from Equation (4.1) is virtually the average permeability for the total

matrix bulk including inorganic and organic grids. It does account the shape factor effect for matrix because the matrix size cannot change it at all.

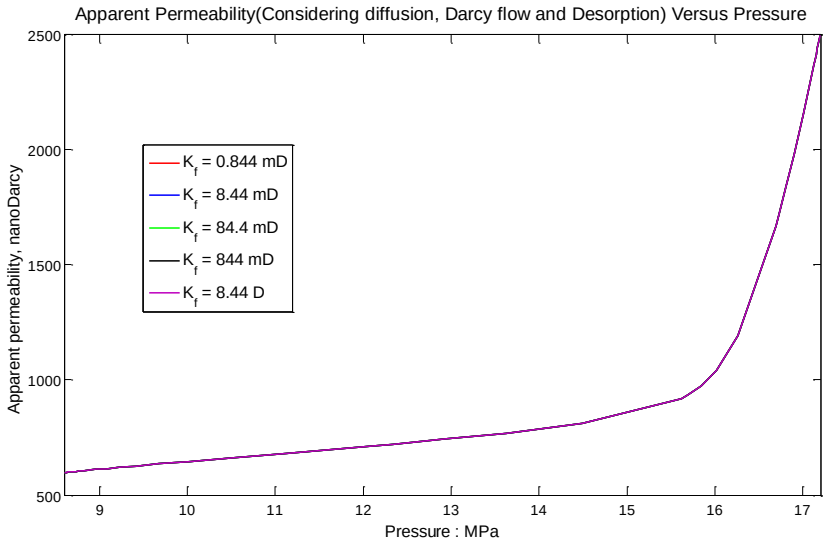

Fig. 4.3—Apparent permeability as a function of pressure with different fracture permeability

4.2 Upscaling with a Triple Permeability Simulation

For the results of the above modeling effort to be useful, the dynamic apparent permeability is further upscaled to a realistic single well model in a commercial simulator (Coats et al. 2003) with multiple fractures are shown in **Fig. 4.4**. As shown in the figure, the well is approximately 5000 feet long with five hydraulic fractures distributed each 1000 feet along the well's length. The width of the simulation model is 3000 feet with a constant reservoir thickness of 500 feet. The first level grid is a three-dimensional system with 30 blocks in the x-direction, 60 blocks in the y-direction, and

10 blocks in the z-direction for a total of 18,000 cells. Local grid refinement is further utilized to better capture the hydraulic fractures by reducing the grid in the y-direction to approximately 5 feet at the fracture locations as shown in **Fig. 4.5**. Three separate porosity systems are simulated here – fracture including hydraulic and natural fractures, organic matrix (kerogen), and finally inorganic matrix. Since the hydraulic fractures and the natural fractures exist at separate grid locations, a single porosity type is used for those fractures. Static permeabilities in the matrix are varied over a range of 50 to 2500 nanodarcies as described below. To capture the dynamic permeability effect of **Fig. 4.1**, pressure-dependent modifications are made to a case which causes the apparent matrix permeability to vary with average matrix block pressures similar to that shown in **Fig. 4.1**. Desorption in kerogen is treated using the technique of Seldle and Arri (1990). Parameters for the desorption are the same as those discussed above to yield an AGWP about 20%. The well is simulated with a maximum rate of 10 MMSCF/d and a minimum bottom-hole pressure of 1247 psia (about 8.6MPa). Initial reservoir properties are 15% water saturation and an initial reservoir pressure of 2495 psia (17.2MPa). Gas properties are derived from correlations for a dry gas. The porosity of the natural fractures is limited to the refined grid area of the stimulated reservoir volume as shown in **Fig. 4.4**. Similarly the hydraulic fracture is confined to a single set of grid blocks extending from the well with a fracture half-length of 1200 feet. Hydraulic fracture permeability and porosity are set to 500md and 0.9, respectively while for the natural fractures values of 10,000 nanoDarcies and 0.02 are used for the permeability and porosity.

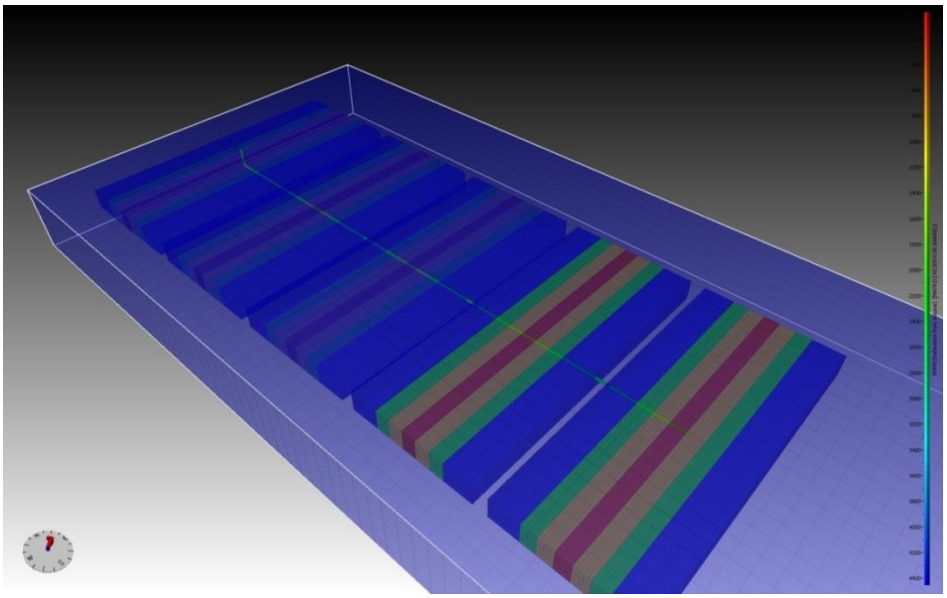

Fig. 4.4—Single Horizontal well with multiple fractures used for upscaled triple permeability simulations

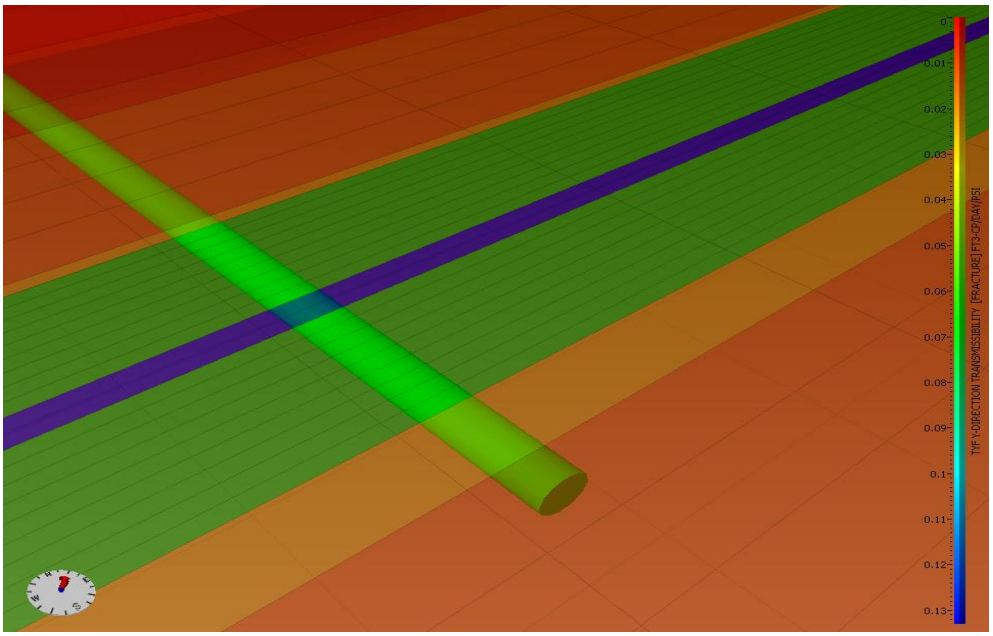

Fig. 4.5—Triple permeability simulation model showing fine grid detail

Simulations are performed with a triple permeability model in which all fractures, inorganic, and organic pore systems are allowed to flow among themselves and between different porosity types. This is different from a MINC or multiple-porosity model in which only the fluids in the fractures are allowed to flow in the fracture network. The well is produced for 30 years with the results shown in **Fig. 4.6** to **Fig. 4.8**.

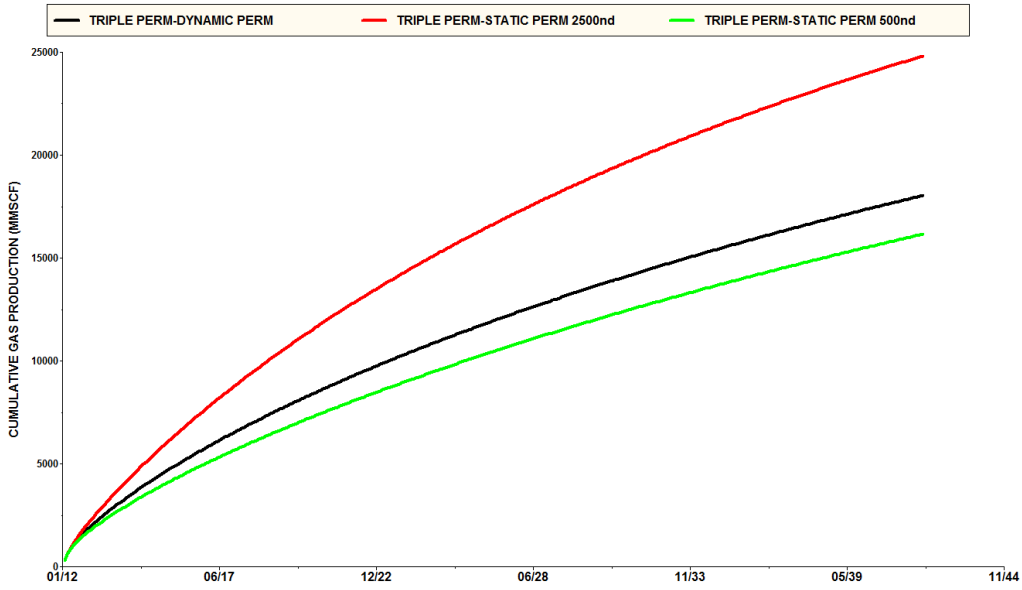

Fig. 4.6—Comparison of different matrix treatments for single horizontal well case

Fig. 4.6 shows the results of three different simulations. The black line represents the case in which the apparent permeability of the matrix is dynamically modified with average matrix block pressure as described above. The green line represents the case for a static apparent permeability of 500 nanodarcies (lower limit) and the red line

represents the static case for 2500 nanodarcies (upper limit). The results in **Fig. 4.6** indicate that, as expected, the dynamic permeability case falls between the maximum and minimum static permeability cases. The dynamic results are closer to the minimum static case due to the rapid falloff in the apparent permeability with average matrix pressure as shown in **Fig. 4.1** from the micro-scale model.

Fig. 4.7 shows the additional results of a low permeability (50 nanodarcies, intrinsic permeability in shale matrix), non-diffusive case. Also presented is a triple porosity case with dynamic apparent permeability in which only the fracture fluids are allowed to flow among other fractures. The blue line for the 50nd matrix permeability is slightly higher than the triple porosity (not permeability) results shown in pink. This indicates that even without diffusive flow, intra-matrix flow has some contribution to the production. The results for the triple porosity case in **Fig. 4.7** show much lower gas production when compared to the triple permeability cases indicating that intra-matrix flow is an important part of the mechanism that must be captured when diffusion in organic matter is considered in the transport process.

The results of **Fig. 4.7** tend to indicate that given certain characteristics of the shale matrix, it might be possible to simulate the gas production process simply by using a static permeability intermediate to the maximum and minimum static values. Unfortunately, this does not appear to be the case as shown in **Fig. 4.8** in which a single static value (875 nanoDarcy) cannot model the entire time period of the simulation.

Simulation times to achieve these results were moderate taking only a few minutes of CPU time per 20 year simulation.

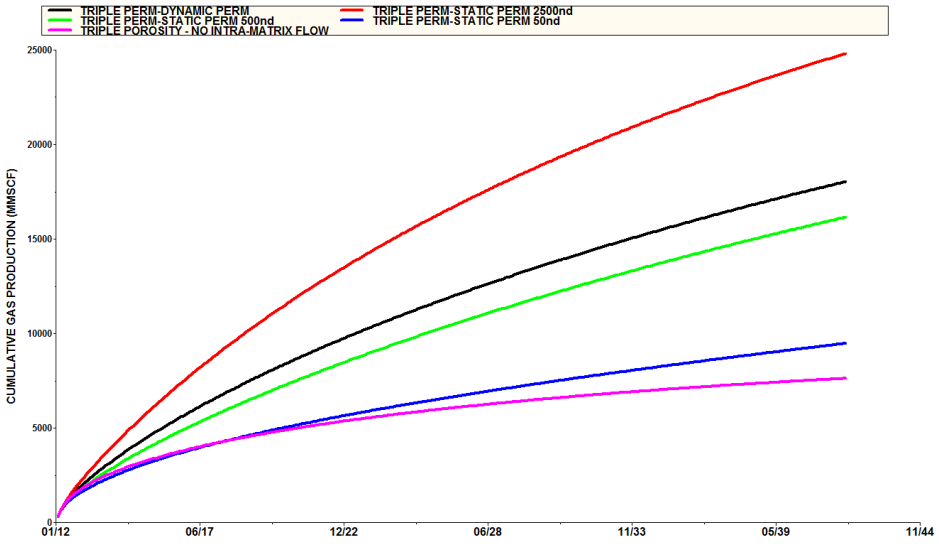

Fig. 4.7—Comparison of static and dynamic permeability treatments in single horizontal well simulation

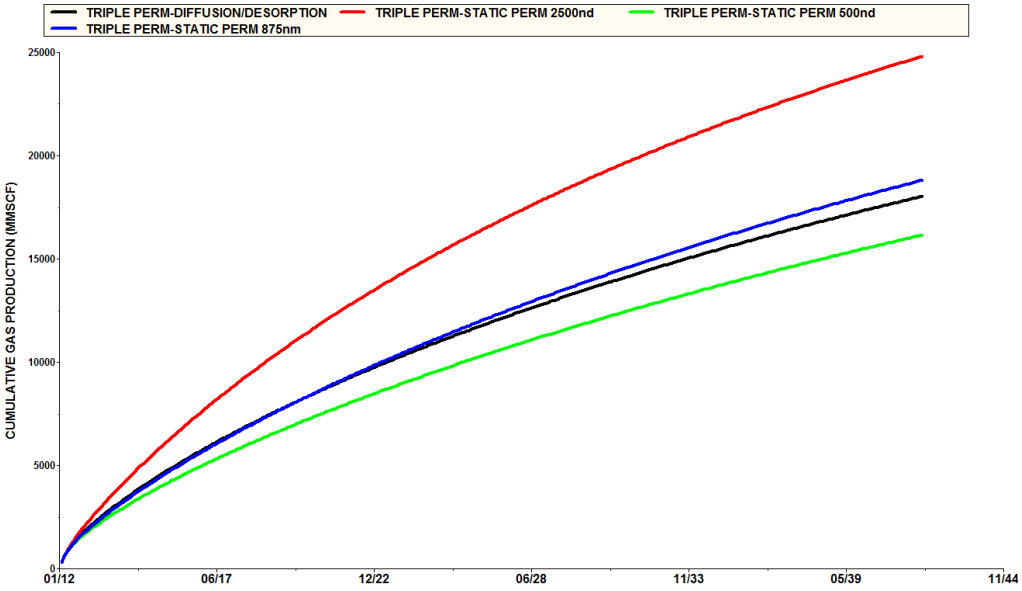

Fig. 4.8—Comparison of static and dynamic permeability treatments in single horizontal well simulation

4.3 Conclusions

This Chapter establishes a workflow to upscale the micro-scale model to a realistic reservoir model. Through analysis, the apparent permeability defined in this research work has little to do with desorption, fracture permeability and matrix size, but is related to average matrix pressure, matrix permeability and diffusion. Through applying the dynamic apparent permeability curve in a realistic reservoir model, diffusion, Darcy flow and transient effect between matrix and fracture could be taken into account.

CHAPTER V

CONCLUSIONS

The research work focuses on the three main issues proposed in Chapter I, and establishes a complete workflow from micro-scale to reservoir scale simulation. The main conclusions for the research work are shown as follows.

(1) A Micro-Scale Model with natural fractures and shale matrix subdivided into three random distributed continua and considering Darcy flow, Fickian diffusion and desorption in kerogen shows results which are consistent with existing data.

(2) With a considerable adsorbed gas weight percentage in shale matrix, gas desorption from kerogen provides more gas in place and sustains a much greater cumulative gas rate and slightly higher average matrix pressure, however, desorption does little to improve the gas drainage capacity (similar to productivity index) and does not influence the apparent permeability defined in this research work.

(3) Diffusion cannot be neglected and is crucial to produce gas in the nanopores in kerogen. Diffusion is fairly effective in enhancing the gas drainage capacity and the apparent permeability.

(4) Darcy flow, diffusion and desorption occur sequentially in the Micro-Scale Model. The latter two mechanisms are strengthened at the later time or lower

average pressure in the matrix bulk because Darcy flow and free gas release dominate the early period.

(5) The difference between the Micro-Scale Model and a traditional Dual Porosity Model with the same pore volume is significant: the former takes into account diffusion and desorption so that the system becomes more producible with subsequent faster pressure drop.

(6) With a constant TOC content in shale, different random distributions of kerogen have a neglectable difference in the global gas flow behavior from the shale matrix bulk to the natural fractures.

(7) Higher TOC content in the shale effectively increases gas in place due to more adsorbed gas and free gas. Higher TOC content also magnifies the effect of diffusion in the kerogen.

(8) The apparent permeability is related to matrix pressure, matrix permeability, diffusion and Darcy flow, but has little to do with fracture permeability, matrix grid size, and desorption.

(9) Upscaling to a reservoir scale model with multiple fractures shows results which indicate that a triple permeability model allowing intra-matrix flow is required to adequately simulate the gas recovery observed in the micro-scale models. Dynamic apparent permeability in the matrix is indispensable in correctly simulating the micro-scopic effects.

REFERENCES

Andrade, J., Civan, F., Devegowda, D. et al. 2011. Design and Examination of Requirements for a Rigorous Shale-Gas Reservoir Simulator Compared to Current Shale-Gas Simulator. Paper presented at the North American Unconventional Gas Conference and Exhibition, The Woodlands, Texas, USA. Society of Petroleum Engineers SPE-144401-MS. DOI: 10.2118/144401-ms.

Beskok, A. and Karniadakis, G.E. 1999. A Model for Flows in Channels, Pipes, and Ducts at Micro and Nano Scales. *Microscale Thermophys Eng.* **3** (1): 43-77.

Civan, F. 2010. Effective Correlation of Apparent Gas Permeability in Tight Porous Media. *Transport in Porous Media* **82** (2): 375-384. DOI: 10.1007/s11242-009-9432-z

Civan, F., Rai, C., and Sondergeld, C. 2011. Shale-Gas Permeability and Diffusivity Inferred by Improved Formulation of Relevant Retention and Transport Mechanisms. *Transport in Porous Media* **86** (3): 925-944. DOI: 10.1007/s11242-010-9665-x

Clarkson, C.R., Nobakht, M., Kaviani, D. et al. 2012. Production Analysis of Tight-Gas and Shale-Gas Reservoirs Using the Dynamic-Slippage Concept. *SPE Journal* **17** (1): pp. 230-242. DOI: 10.2118/144317-pa

Coats, B.K., Fleming, G.C., Watts, J.W. et al. 2003. A Generalized Wellbore and Surface Facility Model, Fully Coupled to a Reservoir Simulator. Paper presented at the SPE Reservoir Simulation Symposium, Houston, Texas. Copyright 2003, Society of Petroleum Engineers Inc. 00079704. DOI: 10.2118/79704-ms.

Cui, X., Bustin, A.M.M., and Bustin, R.M. 2009. Measurements of Gas Permeability and Diffusivity of Tight Reservoir Rocks: Different Approaches and Their Applications. *Geofluids* **9** (3): 208-223. DOI: 10.1111/j.1468-8123.2009.00244.x

Curtis, M.E., Ambrose, R.J., and Sondergeld, C.H. 2010. Structural Characterization of Gas Shales on the Micro- and Nano-Scales. Paper presented at the Canadian Unconventional Resources and International Petroleum Conference, Calgary, Alberta, Canada. Society of Petroleum Engineers SPE-137693-MS. DOI: 10.2118/137693-ms.

Curtis, M.E., Sondergeld, C.H., Ambrose, R.J. et al. 2012. Microstructural Investigation of Gas Shales in Two and Three Dimensions Using Nanometer-Scale Resolution Imaging. *AAPG Bull.* **96** (4): 665-677. DOI: 10.1306/08151110188.

Ertekin, T., King, G.A., and Schwerer, F.C. 1986. Dynamic Gas Slippage: A Unique Dual-Mechanism Approach to the Flow of Gas in Tight Formations. *SPE Formation Evaluation* **1** (1): 43-52. DOI: 10.2118/12045-pa

Freeman, C., Moridis, G.J., Michael, G.E. et al. 2012. Measurement, Modeling, and Diagnostics of Flowing Gas Composition Changes in Shale Gas Wells. Paper presented at the SPE Latin America and Caribbean Petroleum Engineering Conference, Mexico City, Mexico. Society of Petroleum Engineers SPE-153391-MS. DOI: 10.2118/153391-ms.

Hill, D.G. and Nelson, C.R. 2000. Gas Productive Fractured Shales – an Overview and Update. *Gas TIPS*, 4-13.

Hoteit, H. and Firoozabadi, A. 2006. Numerical Modeling of Diffusion in Fractured Media for Gas Injection and Recycling Schemes. Paper presented at the SPE Annual Technical Conference and Exhibition, San Antonio, Texas, USA. Society of Petroleum Engineers SPE-103292-MS. DOI: 10.2118/103292-ms.

Hudson, J.D., Civan, F., Michel, G. et al. 2012. Modeling Multiple-Porosity Transport in Gas-Bearing Shale Formations. Paper presented at the SPE Latin America and Caribbean Petroleum Engineering Conference, Mexico City, Mexico. Society of Petroleum Engineers SPE-153535-MS. DOI: 10.2118/153535-ms.

Javadpour, F. 2009. Nanopores and Apparent Permeability of Gas Flow in Mudrocks (Shales and Siltstone). *Journal of Canadian Petroleum Technology* **48** (8): 16-21. DOI: 10.2118/09-08-16-da

Javadpour, F., Fisher, D., and Unsworth, M. 2007. Nanoscale Gas Flow in Shale Gas Sediments. *Journal of Canadian Petroleum Technology* **46** (10). DOI: 10.2118/07-10-06

King, G.E. 2010. Thirty Years of Gas Shale Fracturing: What Have We Learned? Paper presented at the SPE Annual Technical Conference and Exhibition, Florence, Italy. Society of Petroleum Engineers SPE-133456-MS. DOI: 10.2118/133456-ms.

Loucks, R.G., Reed, R.M., Ruppel, S.C. et al. 2012. Spectrum of Pore Types and Networks in Mudrocks and a Descriptive Classification for Matrix-Related Mudrock Pores. *AAPG Bulletin* **96** (6): 1071-1098. DOI: 10.1306/08171111061

Odusina, E.O., Sondergeld, C.H., and Rai, C.S. 2011. An Nmr Study of Shale Wettability. Paper presented at the Canadian Unconventional Resources Conference, Alberta, Canada. Society of Petroleum Engineers SPE-147371-MS. DOI: 10.2118/147371-ms.

Passey, Q.R., Bohacs, K., Esch, W.L. et al. 2010. From Oil-Prone Source Rock to Gas-Producing Shale Reservoir – Geologic and Petrophysical Characterization of Unconventional Shale-Gas Reservoirs. Paper presented at the International Oil and Gas Conference and Exhibition in China, Beijing, China. Society of Petroleum Engineers SPE-131350-MS. DOI: 10.2118/131350-ms.

Seldle, J.P. and Arri, L.E. 1990. Use of Conventional Reservoir Models for Coalbed Methane Simulation. Paper presented at the Annual Technical Meeting, Calgary, Alberta. Petroleum Society of Canada PETSOC-90-118. DOI: 10.2118/90-118.

Shabro, V., Torres-Verdin, C., and Javadpour, F. 2011. Numerical Simulation of Shale-Gas Production: From Pore-Scale Modeling of Slip-Flow, Knudsen Diffusion, and Langmuir Desorption to Reservoir Modeling of Compressible Fluid. Paper presented at the North American Unconventional Gas Conference and Exhibition, The Woodlands, Texas, USA. Society of Petroleum Engineers SPE-144355-MS. DOI: 10.2118/144355-ms.

Shabro, V., Torres-Verdin, C., and Sepehrnoori, K. 2012. Forecasting Gas Production in Organic Shale with the Combined Numerical Simulation of Gas Diffusion in Kerogen, Langmuir Desorption from Kerogen Surfaces, and Advection in Nanopores. Paper presented at the SPE Annual Technical Conference and Exhibition, San Antonio, Texas, USA. Society of Petroleum Engineers SPE-159250-MS. DOI: 10.2118/159250-ms.

Wang, F.P. and Reed, R.M. 2009. Pore Networks and Fluid Flow in Gas Shales. Paper presented at the SPE Annual Technical Conference and Exhibition, New Orleans, Louisiana. Society of Petroleum Engineers SPE-124253-MS. DOI: 10.2118/124253-ms.

Yan, B., Killough, J., Wang, Y. et al. 2013b. Novel Approaches for the Simulation of Unconventional Reservoirs. Paper presented at the Unconventional Resources Technology Conference, Denver, Colorado, USA. SPE, AAPG, SEG URTeC 1581172.

Yan, B., Wang, Y., and Killough, J. 2013a. Beyond Dual-Porosity Modeling for the Simulation of Complex Flow Mechanisms in Shale Reservoirs. Paper presented at the 2013 SPE Reservoir Simulation Symposium, The Woodlands, TX, USA. Society of Petroleum Engineers SPE-163651-MS. DOI: 10.2118/163651-ms.

Ziarani, A. and Aguilera, R. 2012. Knudsen's Permeability Correction for Tight Porous Media. *Transport in Porous Media* **91** (1): 239-260. DOI: 10.1007/s11242-011-9842-6